Master Degree in Electric Engineering
Propulsion of Hybrid and Electric Vehicles

Report

Alex AIELLO - 336698
Giuseppe MENGA - 324849
Prof. Paolo Guglielmi
A.Y. 2024/2025

Contents

1 Part 1: the Vehicle **1**
1.1 Vehicle choice and specification of usage 1
1.2 Hybridization type (electro-thermal) and motivations 2
1.3 Vehicle performance specifications 3
1.3.1 Problem definition data as given by the teacher and integrations of personal choices 3
1.4 Efficiency estimation of the various systems composing the Traction-Line 3
1.5 Forces evaluation in the vehicle dynamic 4
1.5.1 Aerodynamic Resistance 4
1.5.2 Rolling Resistance 6
1.5.3 Slope 6
1.5.4 Acceleration 6
1.5.5 Total Resistance Force 6
1.6 Continuous torque at wheel specification for maximum slope 7
1.7 Energetic evaluations if the chosen reference standard cycle 9
1.7.1 WLTC 11
1.7.2 Specific cycle 14
1.8 Energetic evaluations in specific conditions 16
1.8.1 Autonomy estimation 16
1.8.2 Maximum acceleration 17
1.9 Simulation in Simulink 18
1.10 Power and Energy specifications of the various components of the Electric Traction Line 20

2 Part 2: the Specifications in tabular form **22**
2.1 Traction storage system 22
2.1.1 Cell specifications 24
2.1.2 Structural Specifications 25
2.1.3 Electric Specifications 25
2.1.4 Energetic Specifications 25
2.1.5 Mechanical Specifications 26
2.1.6 Functions Specifications 26
2.1.7 Control Specifications 27
2.2 Auxiliaries e Services 27
2.2.1 Macro Consumption in LV 27
2.2.2 Macro Consumption 28
2.3 Power Electronics 28
2.3.1 Structural Specifications of the Traction Converter 28

2.3.2 Electrical Specifications of the Traction Converter 28
2.3.3 Energetic Specifications of the Traction Converter 29
2.3.4 Mechanical Specifications of the Traction Converter 29
2.3.5 Sensors in the traction converter 29
2.3.6 Control section of the traction converter 30
2.3.7 Specification of the DC/DC Converter 30
2.4 Charging system specifications 31
2.4.1 External charging system 31
2.4.2 On board charging system 31
2.4.3 Charging time 31
2.5 Electric Machine 32
2.5.1 Electric and Energetic Specifications of the Electric Machine . . . 32
2.5.2 Mechanical Specifications of the Electric Machine 33
2.5.3 Sensors for the electric machine 33
2.6 Transmission 34
2.7 Cooling System 34
2.7.1 Battery Cooling System 34
2.7.2 Inverters and motors cooling system 35

3 Part 3: The Design 37
3.1 The storage system 37
3.1.1 Protection elements 40
3.1.2 Over-current 40
3.1.3 Main Relays (AIR) selection 43
3.1.4 High Voltage harness and connectors 44
3.1.5 Sensors 45
3.1.6 BMS - Battery Management System 48
3.1.7 Pre-charge Circuit sizing 49
3.2 Traction Motor 50
3.2.1 External Dimensions 53
3.2.2 Sensor 54
3.2.3 Transmission 56
3.2.4 Connectors and Cables 56
3.3 Power Electronics 58
3.3.1 Inverters 59
3.3.2 Design of LC Filter between Battery and Inverter 61
3.3.3 Inverter Losses 63
3.3.4 Capacitor choice 64
3.3.5 Sensors 67
3.3.6 High Voltage to Low Voltage DC/DC Converter 69
3.3.7 HV/HV DC/DC Converter for Battery Interface 71
3.3.8 On-Board Charger 73
3.4 Charging 74
3.5 Cooling circuit 76
3.5.1 Low Temperature loop - Battery cooling 77
3.5.2 High Temperature loop - Inverters and motors cooling 79

Chapter 1

Part 1: the Vehicle

1.1 Vehicle choice and specification of usage

The mission of this project work is to size and prepare a utility vehicle for medium-duty transport along rural and hilly roads in southern Italy, specifically covering the route from Monopoli to Alberobello. This route, which spans approximately 32 km, includes both paved and unpaved roads and passes through a region characterized by agriculture, tourism, and small-scale construction activities. The goal is to provide reliable transport support for goods such as farming equipment, construction tools, or tourist-related materials between the coastal area and the inland town. To meet these needs, we selected the Toyota Hilux 2.4 D-4D 4x4 Double Cab [1], a robust and versatile pickup capable of ensuring load capacity, off-road performance, and passenger comfort for mixed-use applications, as shown in Fig. 1.2 and Table 1.1 for the principal vehicle parameters.

Figure 1.1: Picture of the vehicle

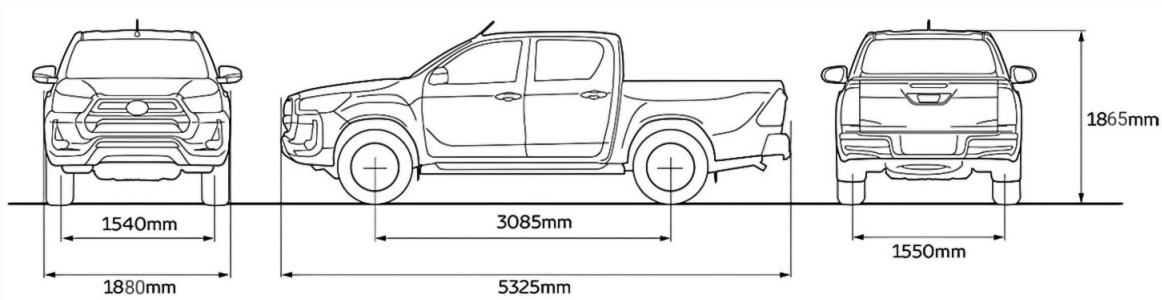

Figure 1.2: Schematic dimension of the vehicle

Table 1.1: Toyota Hilux 2.4 D-4D 4x4 double cab

Vehicle Name		
Heigh	1.865	m
Lenght	5.325	m
width	1.880	m
Wheel Diameter	0.432	m
Fuel Tank	80	l
Frontal Area	3.32	m^2
Boot Volume	1.132	m^3
Weight	3210	kg
Volume	3.53	m^3

1.2 Hybridization type (electro-thermal) and motivations

The chosen version of the Toyota Hilux is the 2.4 D-4D 4x4 double cab, it has an internal combustion engine (ICE) that has a maximum power of 110 kW (150 HP) and a maximum torque of 400 Nm (at 1600-2000 rpm). The goal of the project is to completely electrify the vehicle, removing the internal combustion engine plus the fuel tank and replacing them with a full electrical powertrain. Moreover, two possible configurations are going to be exploited in the second chapter of the report:

- Two electrical machines for the two axles;
- Four electrical machines, one per each wheel.

The first configuration would be preferable from a cost point of view, with fewer components, the chance of failures is reduced, the routing of the TS harness, cooling is simpler and the majority of the masses are all on the sprung mass which enhances the dynamic behaviour of the vehicle, especially allowing an easier neutral distribution of the mass which are closer to the centre of gravity of the vehicle. On the other hand, the second configuration would reduce the number of necessary components. In this specific configuration, the differential would be avoided and can be replaced via software by means of a torque vectoring strategy. In addition, the necessity of smaller e-motors in terms of power and torque will simplify the choice of the model, enlarging the number of possible manufacturers. The main reason to switch to a full-electric vehicle from an OEM point

of view is to line up with the direction imposed by the European union, to reduce the CO_2 emissions produced by transports.

1.3 Vehicle performance specifications

As mentioned in the previous paragraphs, all the components for the combustion model have been removed and all the ones necessary to electrify the pick-up have been added. As already seen, this affected mainly the weight and, consequently, also the dynamic performance of the vehicle. In particular, in the table 1.2 we compare the performances between the two models. The autonomy value of the BEV configuration is evaluated by means of a WLTC cycle.

Table 1.2: Vehicle performance

Vehicle Performances	BEV	ICE	
Autonomy	300	842	km
Maximum Speed	175	170	km/h
Maximum Continuous Slope	25	-	$^\circ$
Maximum Slope	45	-	$^\circ$
0-50 km/h	2.21	-	s
0-100 km/h	7.51	13.2	s
Acceleration	6.81	-	m/s^2
Emissions CO_2	0	243	g/km

1.3.1 Problem definition data as given by the teacher and integrations of personal choices

In this section, some considerations on common specifications for the electric Toyota Hilux are reported. In particular, the maximum charging power value has been found after research on the charging infrastructures present in the market.

Table 1.3: Common Specifications for an electric Toyota Hilux

Characteristic	**Value**	**Meas. Unit**
Max Power at Wheel	250	kW
Max Charging Power	200	kW
Charging Time	70	min
Battery life time	15	years
Accepted reduction of SoC at end of the life	> 80	%
Expected km Performed in One Year	20000	km

1.4 Efficiency estimation of the various systems composing the Traction-Line

In table 1.4, the efficiency for each component is shown. The considered efficiency of the components are taken considering similar cases of applications, mainly from the

Brusa website. These values will be used for the future calculus, especially for the battery sizing ones.

Table 1.4: The traction line efficiency

System	**Efficiency**
Gear	0.93
Motor	0.96
Inverter	0.97
Battery	0.92
Global	$\simeq 0.79$

1.5 Forces evaluation in the vehicle dynamic

Here, all the forces and the approximation adopted are exploited. In the following table, all the parameters used for the forces estimation are reported. In particular, the forces that need to be estimated are the aerodynamic resistance, the rolling resistance, the slope, the acceleration and finally the value of the total resistance force.

Table 1.5: Parameters for forces estimation

Parameters		
ρ_α	1.225	kg/m^3
C_x	1	
A_f	3.32	m^2
v_{max}	48.6	m/s
C_v	0.022	
g	9.81	m/s^2
m_{eq} *no load*	2887	kg
m_{eq} *full load*	3912	kg
α_{max}	0.432	rad

Before in-depth analysis of the formula used, it is necessary to say a few words about the value of the equivalent mass and how it has been found. The equivalent mass of a vehicle is that related to both the actual mass and the additional inertial effects induced by the rotating components. For the sake of simplicity, only the effect given by the rotation of the wheel is taken into consideration.

$$m_{eq} = \frac{5m}{(D/2)^2}$$

Taking into account the weight values found in the chapter 1.7, we can find the value of the equivalent mass reported on the label 1.5.

1.5.1 Aerodynamic Resistance

$$F_\alpha(v) = \frac{1}{2}\rho_\alpha C_x A_f v^2$$

where:

- ρ_α is the air density in $\frac{kg}{m^3}$;
- C_x is the penetration coefficient;
- A_f is the frontal area of the vehicle, calculated from the geometric dimension;
- v is the speed of the vehicle;

1.5.2 Rolling Resistance

$$F_v = C_v m_{eq} g \cos(\alpha)$$

where:

- m_{eq} is the equivalent mass of the vehicle;
- C_v is the rolling friction coefficient on asphalt with normal tires;
- g is the gravity acceleration;
- α is the angle corresponding to the considered slope;

1.5.3 Slope

$$F_s = m_{eq} g \sin(\alpha)$$

where:

- m_{eq} is the equivalent mass of the vehicle;
- g is the gravity acceleration;
- α is the angle corresponding to the considered slope;

1.5.4 Acceleration

$$F_a = m_{eq} a$$

where:

- m_{eq} is the equivalent mass of the vehicle;
- - a is the acceleration of the vehicle;

1.5.5 Total Resistance Force

$$F_{res}(v, \alpha) = F_v + F_v(\alpha) + F_s(\alpha)$$

1.6 Continuous torque at wheel specification for maximum slope

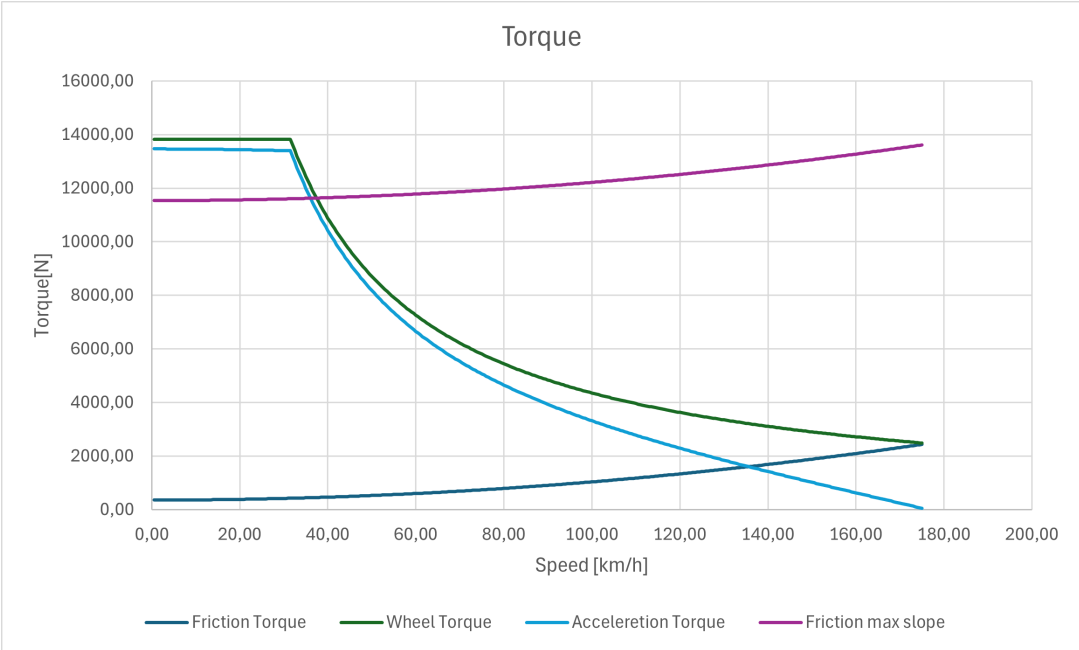

Figure 1.3: Mechanical characteristic - wheel side

Table 1.6: Forces and torque at the wheel

Forces	**Value**	**Meas. Unit**
Rolling Force at Zero Slope	830.9	N
Slope Force at Max Slope	26706.362	N
Aerodynamic Force at Max Speed	4805.25	N
Maximum Total Resistance Force	5636.15	N
Maximum Continuous Wheel Torque	13824.0	Nm

By analysing the previous plot, it might seem that reaching the max speed of the vehicle the line of the wheel Torque and the friction Torque converge to the same value. The following picture is a closer look to the mechanical characteristics of the vehicle at higher speeds (in particular from 150 km/h to 175 km/h). It is possible to notice that the wheel torque line is always above the friction torque one. The closer point between those two lines can be found at the max speed, but the difference among the two stands around $\simeq$ 60Nm.

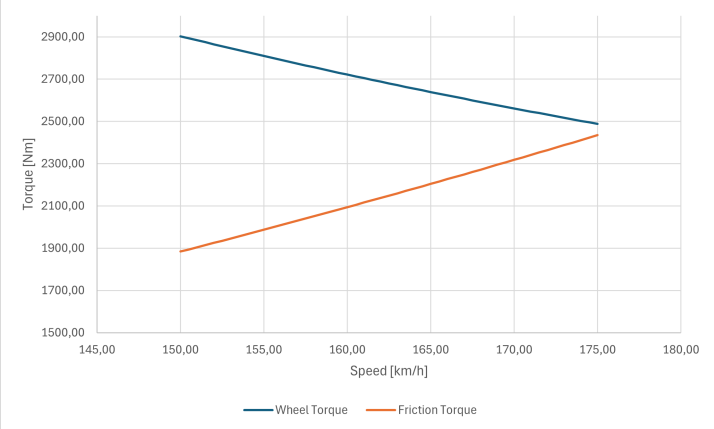

Figure 1.4: Mechanical characteristic high speed - wheel side

In the following graph, the power characteristic of the battery can be evaluated. It is interesting to underline that up to now, the value of the gear ratio for the sake of simplicity has been kept equal to one.

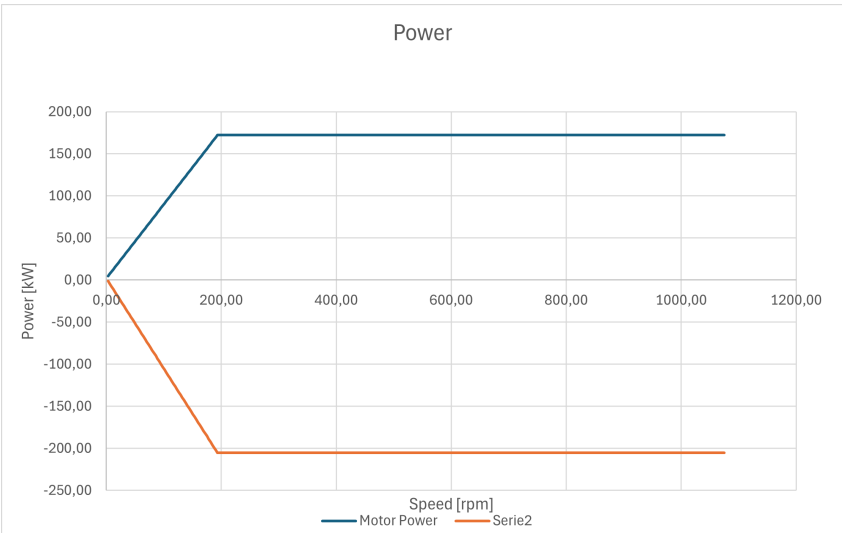

Figure 1.5: Power characteristic - battery side

1.7 Energetic evaluations if the chosen reference standard cycle

In the following chapter, the energetic dimensioning of the battery pack has been done. In particular, the target distance that we wanted to achieve was equal to **300 km**, considering the average consumption in a WLTC cycle. To succeed in this task, different cycles are evaluated:

- **WLTC cycle**, this cycle has replaced the older NEDC. This change was necessary after research done by the Autoclub Germany in 2012 found out that the actual fuel consumption of the cars was 19.6 percent higher than the one present in the datasheet (found by means of the NEDC). The WLTC has been used since 2017 and is able to provide more realistic results thank to its uniformity and closer driving profile to the one of real conditions;

- **Specific cycle**, this specific cycle has been dictated by a personal choice. In particular, we decided to refer this specific cycle to the distance between Monopoli and Alberobello. The distance between these two cities is 16.2 km, bringing the total distance covered in a single cycle to 32.5 km.

The max value of the slope for the specific cycle stands around 42 percent ($\simeq 22°$); meanwhile for the other two cycles the slope is equal to zero.

Regarding the dimensioning of the battery pack, we started with the estimation of the electric vehicle weight, from there we found by means of the WLTC test the necessary amount of energy for the battery pack to satisfy the target autonomy, set equal to 300 km. After finding out the value of the energy required, we found the approximate weight of the battery pack (considering cells with specific energy of 250 Wh/kg). The weight estimation can be found in the following table.

Table 1.7: Removed weight from CV model

Component	**Weight**	**Meas. Unit**
Motor: Diesel, 4 cylinders, 2400 CV	230	kg
Fuel system (full fuel tank)	83.5	kg
exhaust system	18	kg
engine cooling system	18	kg
Car air intake system	4	kg
Alternator and starter	10	kg
Gearbox	65	kg
Car starting battery and ECU	23.8	kg
Total	$\simeq 452.3$	kg

Table 1.8: Added weight for EV model

Component	**Weight**	**Meas. Unit**
eMotor	200	kg
geartrain	80	kg
Battery	750	kg
VCU and charger	10	kg
Cooling system	27	kg
Harness (both LV and HV)	21	kg
Auxiliary systems	15	kg
Total	$\simeq$ 1123	kg

To estimate the weight of the battery pack, an iterative approach was followed. Firstly, we have evaluated the value of necessary energy considering the weight of the CV model. Obtaining the energy value [in kWh] and knowing the value of the specific energy of the cell we wanted to use, we found the first possible weight of the battery pack. After this first phase, we went back to the WLTC cycle and again evaluated the amount of energy necessary. This iterative approach has come to an end once the weight of the battery pack (and consequently, its energy) were compliant with the 300 km, which correspond to the distance target set by us.

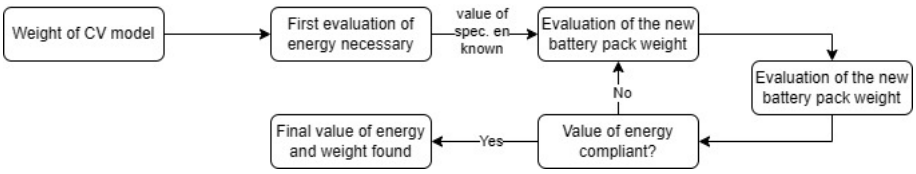

Figure 1.6: Iterative approach to BP weight and energy

At the end of this weight estimation, these are the information that we were able to carry out:

- **No load weight EV** = 2825.64 kg
- **Load capacity** = 1025 kg
- **Total mass EV** = 3850.64 kg

1.7.1 WLTC

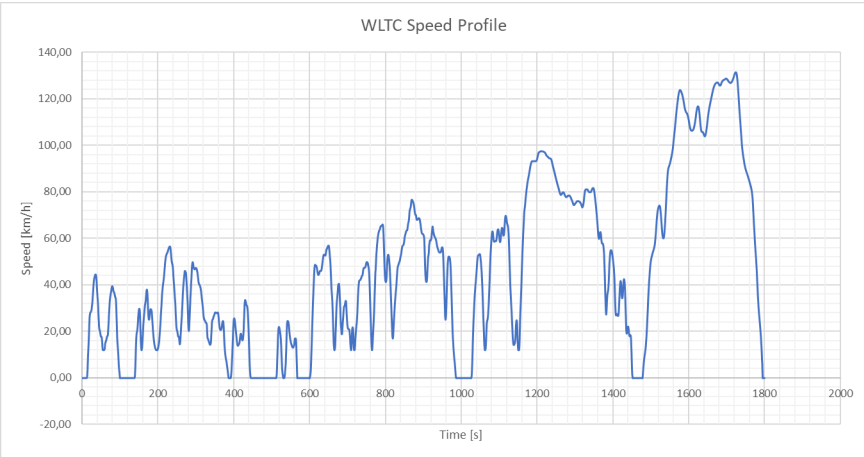

Figure 1.7: WLTC speed profile

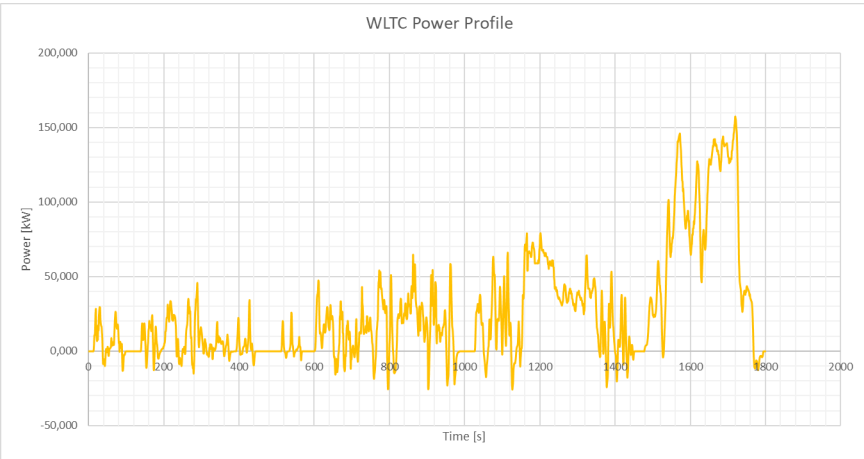

Figure 1.8: WLTC power requested

Taking into account the estimated weight of the EV version, a WLTC cycle was performed. The net energy requested is given by subtraction from the discharge energy and the regenerative braking energy. It is necessary to underline that the amount of braking power regenerated was only the 70 percent of the total power, this was essential to guarantee passengers comfort in all conditions. In addition, when the vehicle is running under 20 km/h no regenerative braking is allowed. All the braking force must come through the mechanical system.

Table 1.9: Energy for a WLTC cycle

	Energy
Regenerative braking	13.45 kWh
No regenerative braking	14.93 kWh

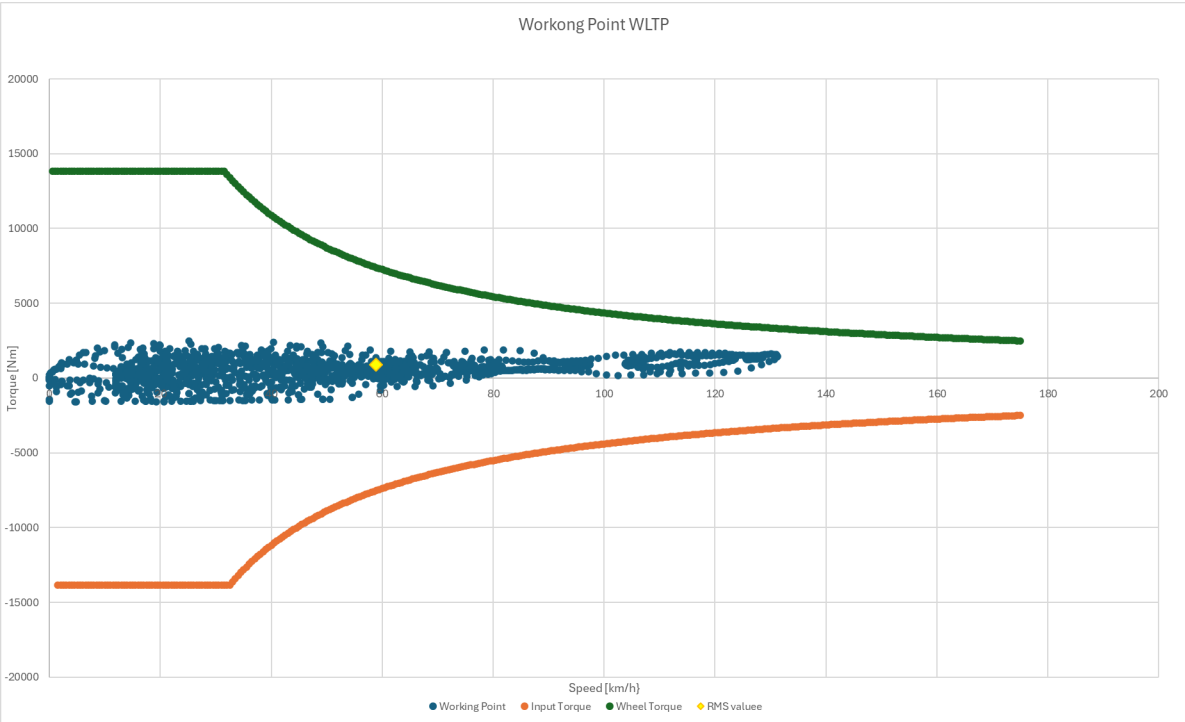

Figure 1.9: WLTC working point - wheels

The total distance of the WLTC test is 23.262 km, to achieve the 300 km of autonomy for the electric vehicle, the cycle must be repeated at least 13 times.

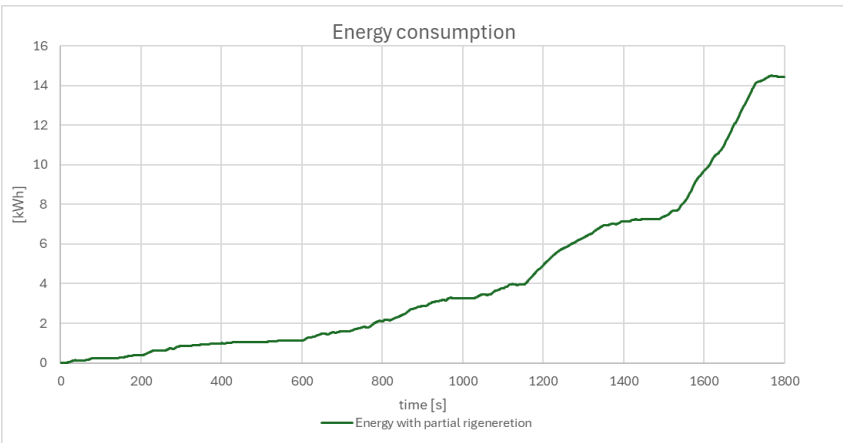

Figure 1.10: WLTC power requested

$$n = eccess(\frac{l}{L}) = eccess(\frac{300}{23.26}) = 13$$

$$E_b = E_{bcycle} * n = 14.45 * 13 = 187.5kWh$$

where:

- n = number of cycles;
- l = length of single WLTC cycle [km];

- L = Distance target set [km];

At the end of the 13 repetitions, the **energy required for the traction system is 187.5 kWh**. On the other hand, it is necessary to also consider the energy necessary for the auxiliaries. The energy necessary is calculated as follows:

$$E_{aux} = \frac{P_{aux} * t_{WLTC} * n}{3600} = \frac{2 * 1800 * 13}{3600} = 13kWh$$

The final value of the necessary energy for the battery pack is given by the sum of these two contributions. The final value of energy is **200 kWh**.

1.7.2 Specific cycle

The specific cycle regards a complete trip from Monopoli to Alberobello, considering also the return. The total length of the cycle is 32.5 km, with a min altitude in Monopoli of 0.9 m and a max one of 419 m. Regarding the slope, the maximum one that we can find in this specific cycle is 41.4%. Considering that the mission is both on urban and extra urban environments but not on highways, we imposed the base speed of the vehicle (at zero slope) equal to 30 km/h. The mass considered for all the calculation is the equivalent one at full load (worst case scenario), founded in the chapter 1.5.

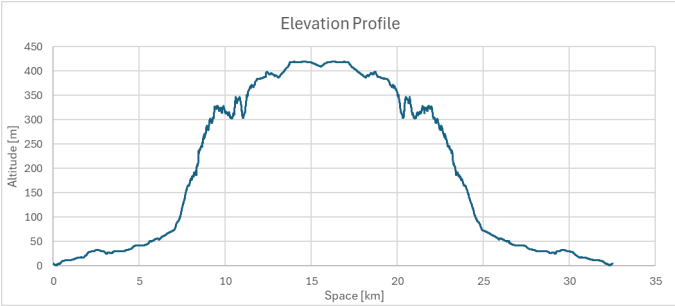

Figure 1.11: Specific cycle altitude variation

For the specific cycle, the same evaluation were made as for the WLTC cycle. However, it is necessary to underline that differently from the WLTC which has zero slope for the whole test, the specific mission has a slope that changes throughout the whole cycle. Below, the plot with the slope behaviour with respect to the distance is reported.

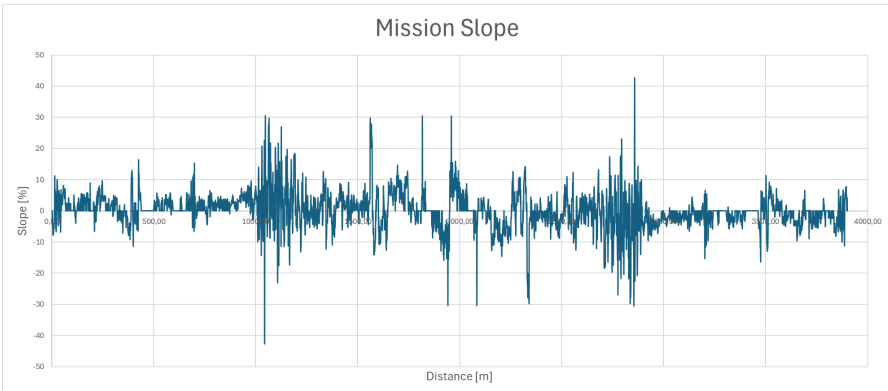

Figure 1.12: Specific cycle slope variation

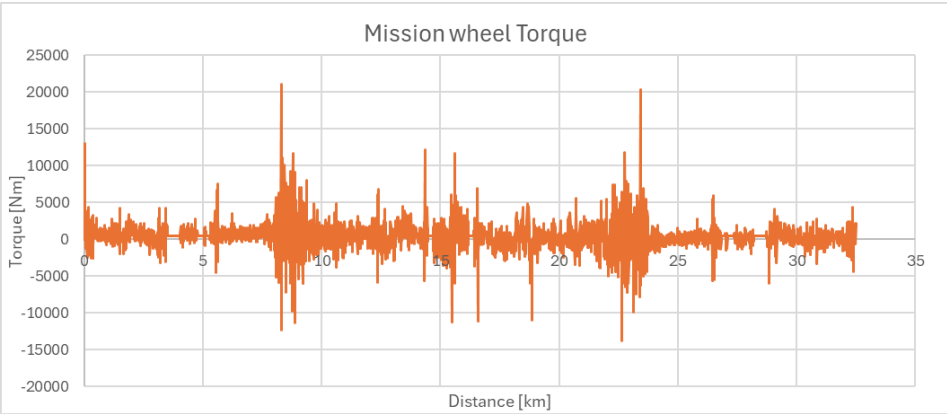

Figure 1.13: Specific cycle torque at wheels

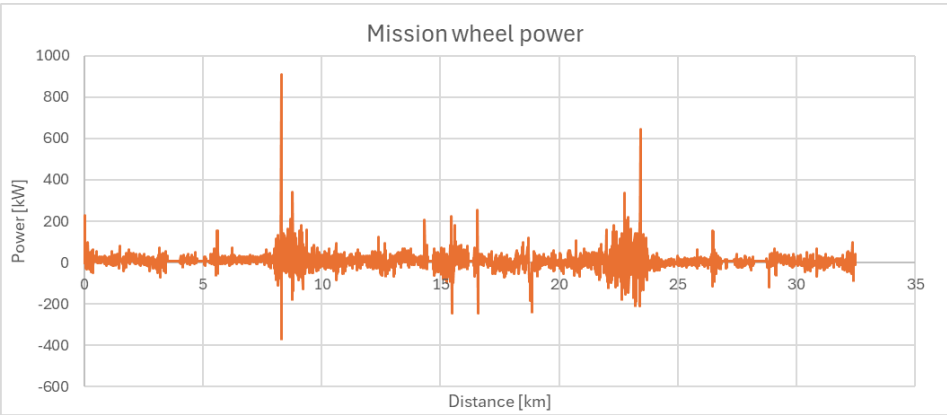

Figure 1.14: Specific cycle power at battery

It is interesting to notice that around the 8 km mark, the power requested is around 900 kW which is unrealistic. Another point in which this happens is around the same distance but in this case in recharge, with the power reaching almost 400 kW. This can be explained by a inaccuracy in the slope levels taken. In fact, all the value of longitude, latitude and altitude are taken from the software **google earth Pro**. However, considering that the max charging power of the electrical motor is 260 kW, the power that could flow in the battery pack is equal to max power in charge multiplied to the efficiencies of the driveline.

$$P_{bat,ch} = P_{mot,ch} * \eta_{mot} * \eta_{inv} * \eta_{bat} - P_{aux} * \eta_{inv}$$
$$= 260 * 0.96 * 0.97 * 0.92 - 2 * 0.97 = 221.15kW$$

For this reason, it is necessary to limit the maximum value of power that can be regenerated. The limit must be equal or below the maximum charging power of the motor. The rest of necessary power to slow down the vehicle must come from the mechanical braking.

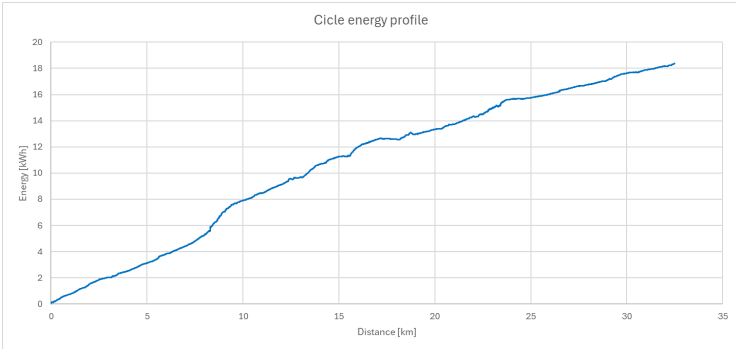

Figure 1.15: Specific cycle energy at battery - fixed

Following the same value of working of the WLTC cycle, the same formulas were used for the energy evaluation.

$$n = eccess(\frac{l}{L}) = eccess(\frac{300}{32.5}) = 10$$

$$E_b = E_{b,cycle} * n = 18.4 * 10 = 184kWh$$

where:

- n = number of cycles;
- l = length of the specific mission cycle [km];
- L = Distance target set [km];

At the end of the 10 repetitions, the **energy required is 184 kWh**. Following the evaluation done for the WLTC cycle, also in this case we should consider the amount of energy necessary for the auxiliaries (equal to 13 kWh). For this reason, the **final value of necessary energy is 197 kWh**.

1.8 Energetic evaluations in specific conditions

In this section will be reported a series of energetic evaluations under different circumstances, in order to better understand the behaviour of the Toyota Hilux with the electric powertrain.

1.8.1 Autonomy estimation

These are the formulas useful to calculate empirically the autonomy of the vehicle:

$$Autonomy(h) = \frac{E_b * \eta_b}{((\frac{P_w}{\eta_c * \eta_m * \eta g}) + P_{aux})}$$

$$Autonomy(km) = Autonomy(h) * speed(km/h)$$

Using Excel, it's possible to represent on a graphic the autonomy of the vehicle depending on the vehicle speed. In addition, the estimation will be performed considering different values of the auxiliaries consumption. In particular, four different case has been examined:

- case 1: electronics plus on-board auxiliaries (200-470 W);
- case 2: headlights, wipers and ventilation (470-930 W);
- case 3: air conditioning, radiator fan and infotainment (930-1400 W);
- case 4: all of the above combined (1400-2000 W);

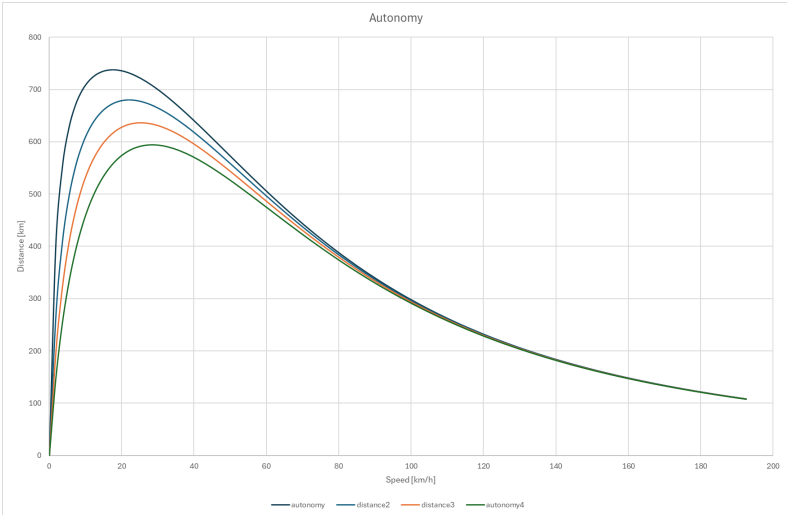

Figure 1.16: Autonomy at different auxiliaries consumption

Referring to the graph above, it is interesting to highlight the speed value at which the maximum autonomy is reached.

Table 1.10: Speed at which max autonomy is achieved

Auxiliaries load	**Max autonomy**	**Vehicle speed**
Case 1	737.89 km	18 km/h
Case 2	679.81 km	21.6 km/h
Case 3	636.85 km	25.2 km/h
Case 4	594.52 km	28.8 km/h

1.8.2 Maximum acceleration

Excel acceleration calculation

$$v_k = v_{k-1} + \frac{F_{d(v_{k-1})} - F_{ad(v_{k-1})}}{m_{eq}} * \Delta t$$

$$F_d = Drivingforce$$

$$F_{ad} = Advancementforce$$

Still considering the Excel simulations, it's possible to evaluate how the vehicle acceleration changes according to the load, considering the maximum slope only for a single case with full load (for the other calculations, the slope is equal to zero).

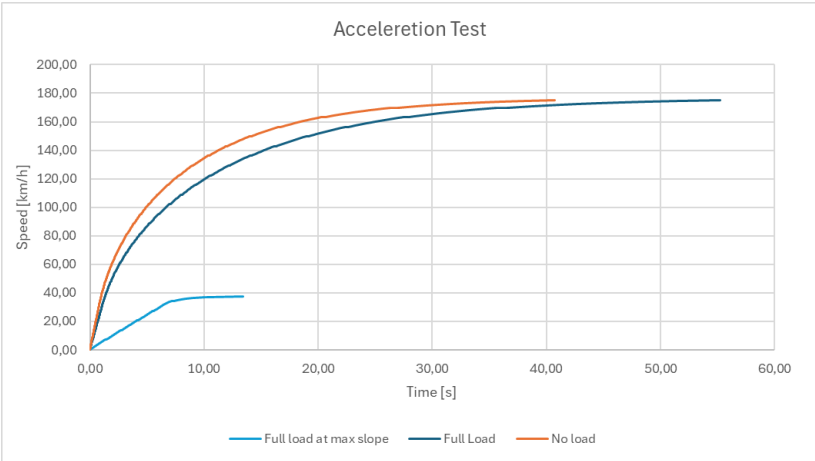

Figure 1.17: Acceleration test at different load values

Referring to the figure above, it's interesting to highlight the time value at which a speed of 100 km/h is reached, according to the different values of the load considered.

Table 1.11: Acceleration 0-100 km/h according to load

Load value	**Time to reach 100 km/h**	**Acceleration**
No load	4.98 s	2.64 m/s^2
Maximum load	6.75 s	1.94 m/s^2

In conclusion, it is possible to notice that at full load and maximum slope the curve stops after 15 seconds. This is in line with the target set by us at the beginning of the dimensioning, where we set at 30 km/h the speed that we wanted to reach at maximum slope. By analysing the graph, we can notice that we are able to reach 37.5 km/h.

1.9 Simulation in Simulink

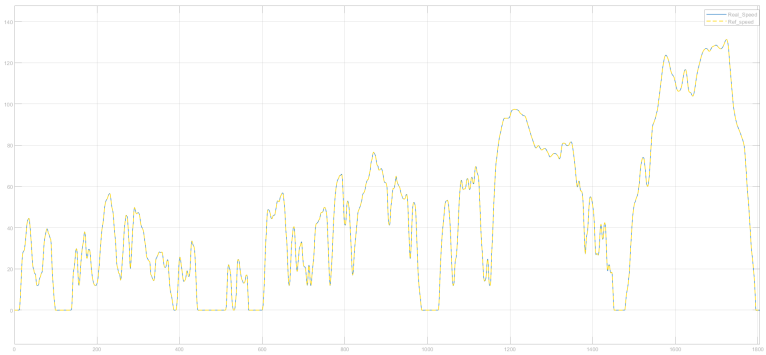

Figure 1.18: WLTC Cycle Excel vs Simulink

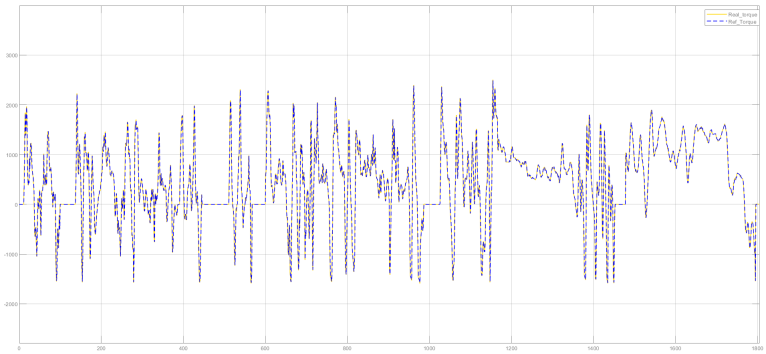

Figure 1.19: WLTC torque at wheels Excel vs Simulink

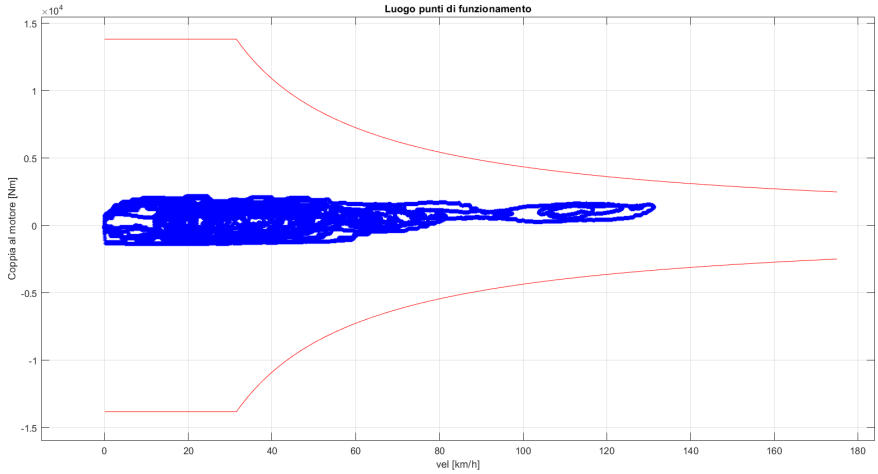

Figure 1.20: Simulink working points for the WLTC cycle

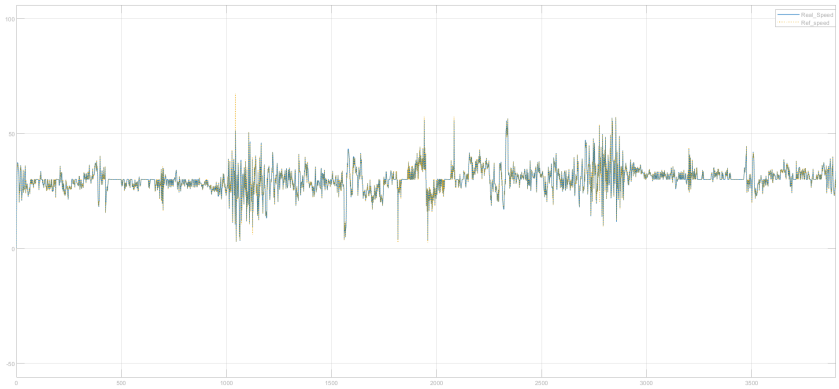

Figure 1.21: Specific speed profile Excel vs Simulink

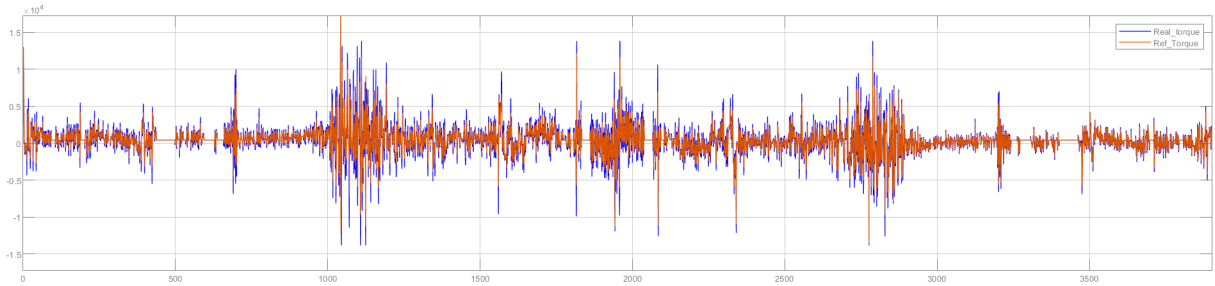

Figure 1.22: Specific cycle torque at wheels Excel vs Simulink

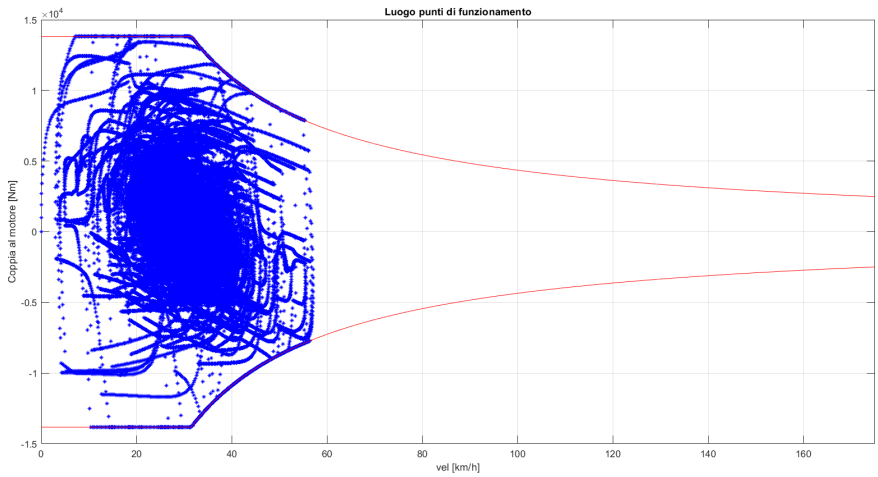

Figure 1.23: Simulink working points for the Specific cycle

Same test as before with comparison with excel calculation

1.10 Power and Energy specifications of the various components of the Electric Traction Line

In order to properly size the electric traction line for the Toyota Hilux 2.4 D-4D 4x4 Double Cab during the rural trip from Monopoli to Alberobello, it is necessary to evaluate the power and energy demands of each component. This evaluation is based on an equivalent mass model and considers both a standardized drive cycle (WLTC) and a specific one adapted to the target route.

Table 1.12 reports the efficiency and energy losses of each component of the traction line — gear, motor, converter, and battery — expressed in terms of mean, RMS, maximum, and energy values for both WLTC and the specific cycle. These values are essential to estimate the thermal and electrical stress on each subsystem.

Table 1.13 provides the power levels required by each component, including mean, RMS, and peak values. These data are fundamental for defining the correct nominal power ratings and ensuring reliable performance across typical and demanding operating conditions.

Table 1.12: Losses of Electric Traction line components.

Components	**gear**	**motor**	**converter**	**battery**
Efficiency	0.93	0.96	0.97	0.92
Mean Losses WLTC [W]	1896	1120	862.5	2484
RMS Losses WLTC [W]	2947	1749	1351	3908
Energy Losses WLTC [Wh]	1.02	0.61	0.47	1.37
Max. Losses WLTC [W]	10190	6066	4690	13590
Mean Losses Spec. Cycle [W]	1886	1079	814.4	2278
RMS Losses Spec. Cycle [W]	3009	1708	1286	3592
Energy Losses Spec. Cycle [Wh]	688	409.53	316.64	917.81
Max. Losses Spec. Cycle [W]	21080	12550	970	28120

Table 1.13: Powers of Electric Traction line components.

Components	**gear**	**motor**	**converter**	**battery**
Mean Power WLTC [kW]	23.46	24.58	25.44	27.92
RMS Power WLTC [kW]	42.02	43.7	45	48.8
Max. Power WLTC [kW]	145.6	151.6	156.3	169.9
Mean Power Spec. Cycle [kW]	0.78	0.89	0.97	1.20
RMS Power Spec. Cycle [kW]	4.16	4.21	4.24	4.38
Max. Power Spec. Cycle [kW]	30.11	31.36	32.33	35.15

Chapter 2

Part 2: the Specifications in tabular form

2.1 Traction storage system

In this part, thanks to the results obtained in section one, it is possible to physically size and choose the new tractive system of the Toyota Hilux, taking into account the cooling of the various components. Considering the high values of torque and power plus the configuration of four wheel drive, we opted to use four different motors (one per each wheel) fed by their own inverter. In this way, we are able to completely remove the necessity of a differential for our car, since the torque repartition is done at control levels through Torque Vectoring. Under these conditions, the schematics of the traction line and the cooling system are reported in the following figures.

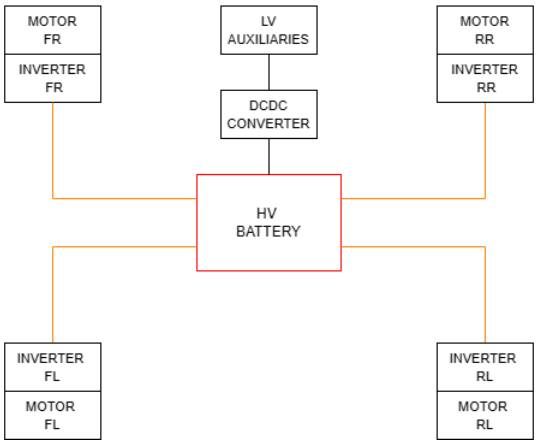

Figure 2.1: Tractive system configuration

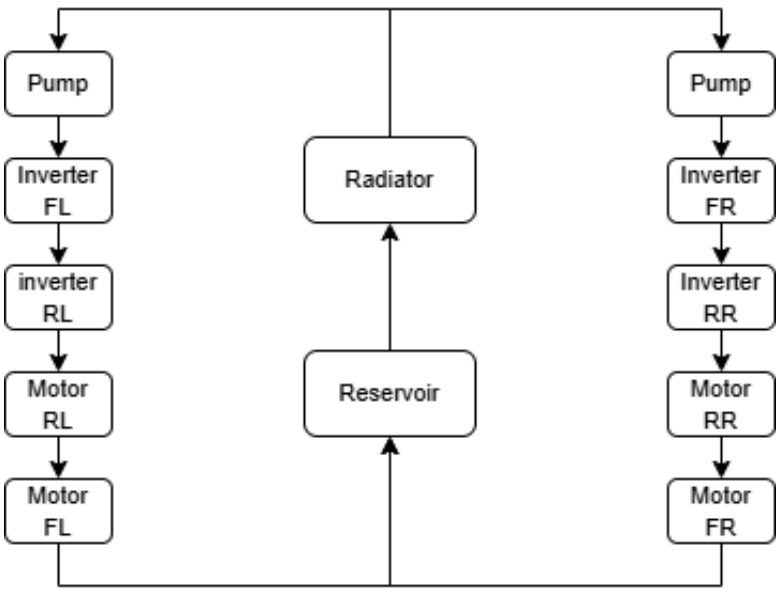

Figure 2.2: Cooling system configuration

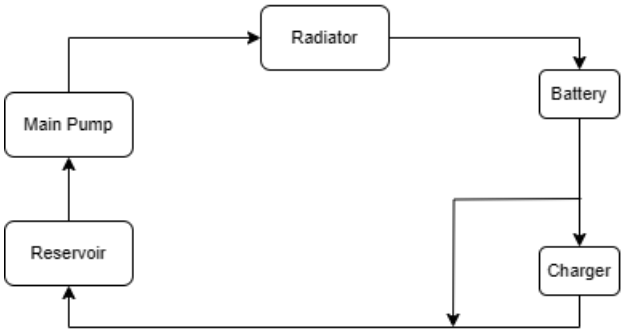

Figure 2.3: Cooling schematic battery and charger

2.1.1 Cell specifications

Table 2.1: Cell Samsung SDI 21700-50E

SDI 21700-50E		
Capacity	4.9	Ah
$I^{max}_{Discharge_{cont}}$	2C - 9.8	A
$I^{max}_{Discharge_{peak}}$	3C - 14.7	A
I^{max}_{Charge}	1C - 4.9	A
V_{nom}	3.6	V
Lower Limit Voltage	4.2	V
Upper Limit Voltage	2.5	V
Weight	68.8	g
Tipology	Cylindrical	
Diameter	20.25	mm
Height	70.8	mm
Volume	0.022	l
Impedance(1kHz AC)	26.5	$m\Omega$
Gravimetric Energy Density	265	Wh/kg
Volumetric Energy Density	719	Wh/l
Volumetric Power Density	2.32	W/l
Charge Temperature Range	0 to +45	$°C$
Discharge Temperature Range	-20 to +60	$°C$

Using a scale, it is possible to see that the cell weight is equal to 68.8 g. Some constant current tests have been performed with the specific cell, to better understand how it behaves with different discharge currents. The results of this test are shown below.

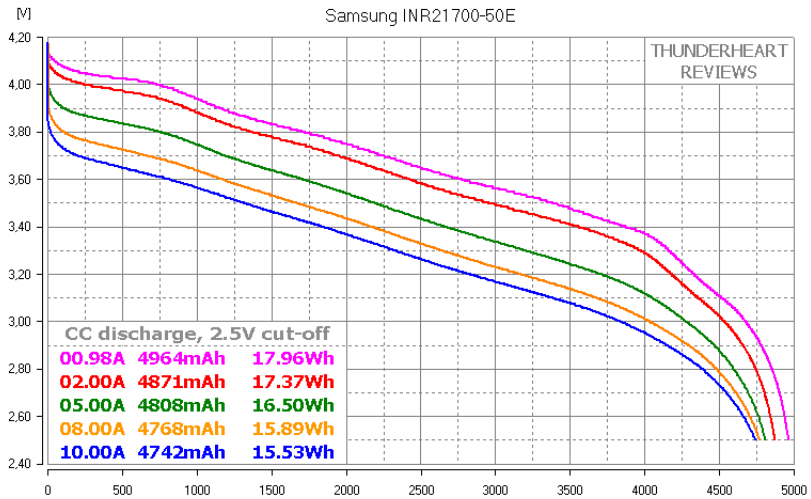

Figure 2.4: Cell constant current tests

It is possible to observe that at maximum continuous discharge current (if kept constant), the value of capacity would still be equal to 4742 mAh. The offset between this value and the nominal one is around 3%.

2.1.2 Structural Specifications

Table 2.2: Structural specification of the storage system

N. Packs	1	
N. modules per pack	12	
N. cells per module	954 - 18s53p	
Net cells weight	746	kg
Net cell volume	278.4	l
Weight	860	kg
Volume	400	l

2.1.3 Electric Specifications

Table 2.3: Electric specifications of the storage system

Voltage Nom.	777.6	V
Maximum Absolute Voltage	907	V
Minimum Absolute Voltage	540	V
Maximum Operative Voltage	900	V
Minimum Operative Voltage	547	V
$\mathbf{I_{disch,max,cont}}$	350 (imposed)	A
$\mathbf{I_{disch,max,peak}}$	540 (imposed)	A
$\mathbf{I_{charge,max}}$	259.7	A
Insulations	1.2	MΩ
IP Class	IP 68	

The value of the maximum peak discharging current has been found as the ratio between the maximum output power of the battery (imposed by us equal to 300 kW) and the minimum operating voltage. The same procedure has been used for the calculation of the maximum continuous discharge current. Instead, the maximum charging current has been found using the value given on the datasheet, multiplying it by the number of cells in parallel.

2.1.4 Energetic Specifications

The energetic specifications are described for the whole mission. The energy consider also the one for the auxiliaries that need to be supplied throughout the whole mission.

Table 2.4: Energetic specifications by the storage system

Min. Energy to be stored	197	kWh
Min. Power in continuous	200	kW
Min. Power in peak	300	kW
peak duration	3	sec
Cooling type	liquid	50 Ethylene Glycol + 50 Water
Fluid flow-rate per module	2.7	l/min
Density ρ	1040	kg/m^3
Specific heat c_p	3.45	kJ/kgK
Working temperature	-20 to +60	$°C$
Charging temperature	0 to +45	$°C$
Pressure drop estimation	0.20	bar
Battery efficiency	92	%
Total Power loss	16	kW

Power losses are calculated considering the battery efficiency, equal to 92%. This bring the total power loss equal to 16 kW. The formula used for the fluid flow-rate is the following one.

$$\dot{V} = Q/(\rho * c_p * \Delta_T)$$

2.1.5 Mechanical Specifications

Table 2.5: Mechanical specifications of the storage system

Maximum effective expected volume	400	l
Maximum expected dimensions	0.4	m^3
Maximum expected weight	860	kg

2.1.6 Functions Specifications

Table 2.6: Storage system operation specifications

Duration in Cycles	> 6000	$cycles$
Duration in kilometers	200000	km
Duration in years (1 cycle per day)	> 16	$years$
MTBF	42000	$hours$
Nominal Current of the fuse	> 400	A
Nominal Voltage of the fuse	1000	V
Breaking Capacity of the fuse	16	kA
Nominal current of the circuit breaker	> 400	A
Nominal voltage of the circuit breaker	1000	V

The "Mean Time Before Failure" (MTBF) is calculated with the following equation:

$$MTBF = \frac{E_{\text{tot,usable}}}{E_{\text{1cycleWLTP}}} \cdot \Delta t_{\text{1,cycleWLTP}} \cdot n^{\circ}_{\text{guaranteed}}$$

2.1.7 Control Specifications

Table 2.7: Control specifications of the storage system

Communication type	CAN	
communication speed	1	$\frac{Mbit}{s}$
Control section power supply	9-16	V
Consumption of the control section	30	W

2.2 Auxiliaries e Services

2.2.1 Macro Consumption in LV

Table 2.8: Macro Consumption in LV

	V	kW	kg
Air conditioning	48	2	20
Power steering	48	1	4
Hydroelectric pump	12	0.5	3
Dashboard lights	12	0.02	0.2
Front and rear windscreen wiper	12	0.1	1
Cockpit light	12	0.02	0.1
Arrow lights	12	0.03	0.3
Positions lights	12	0.02	0.2
Dipped headlights	12	0.07	0.5
Headlights	12	0.1	0.6
Front directional headlights	12	0.06	0.4
Fog lights	12	0.07	0.4
Rear position lights	12	0.02	0.2
Reverse lights	12	0.03	0.2
Intern lights	12	0.01	0.1
Rear directional light	12	0.04	0.3
Licence plate light	12	0.01	0.1
Fan condictioning	12	0.3	1
Horn	12	0.07	0.5
Radio	12	0.1	1
Control Unit	12	0.03	0.5
ABS	12	0.2	2
HVAC Compressor	12	1.5	8
USB Chargers	12	0.02	0.1
Parking sensors	12	0.02	0.2
Camera system	12	0.08	0.5

2.2.2 Macro Consumption

Table 2.9: Macro Consumption in LV and HV

		kW
Total Power in LV	12V	3.42
Total Power in LV	48V	3

Considering all the consumption reported in 2.8 the total power required by auxiliaries is equal to 6.42 kW. This values, reduce the autonomy of the vehicle travelling at 42 km/h constant to 428 km.

2.3 Power Electronics

2.3.1 Structural Specifications of the Traction Converter

The Toyota Hilux EV is equipped with:

- **Four 3-phase voltage source inverters** supplying the individual wheel motors. Each inverter is based on silicon carbide (SiC) MOSFET technology and allows high-frequency switching, high efficiency, and precise torque control for full four-wheel-drive capability;
- **One DC/DC converter** to supply the 12 V auxiliary systems and to recharge the low-voltage battery;

The traction inverters are connected in parallel to the battery pack, which operates with a nominal voltage of up to 900 V.

2.3.2 Electrical Specifications of the Traction Converter

Each inverter module is intended for high-voltage traction applications, exploiting the advantages of silicon carbide (SiC) MOSFETs for high efficiency and fast switching performance. The module features a compact layout with integrated temperature sensing and is designed to be cooled by direct liquid flow.

Type	3-phase full-bridge SiC inverter module
Maximum drain-source voltage	1200 V
Continuous drain current	up to 400 A
Pulsed drain current	up to 800 A
Drain-source on-resistance	2.75–3.70 mΩ @ 25°C, 400 A
Gate-source voltage range	–10 V to +20 V
Stray inductance (typical)	≈8.5 nH
Integrated features	NTC sensor, low-inductive layout
Switching frequency capability	up to 20 kHz
Maximum Output Frequency	1600 Hz

Table 2.10: Preliminary electrical specifications of the SiC traction inverter.

2.3.3 Energetic Specifications of the Traction Converter

Parameter	Value	Unit / Notes
Electric Power Output	> 170	kW
Efficiency (at nominal load)	> 97	%
Estimated Power Losses	< 6	kW
Cooling Type	Liquid	50% Ethylene Glycol + 50% Water
Coolant Inlet Temperature	40–50	°C
Coolant Outlet Temperature	60–70	°C
Coolant Flow Rate	6–10	l/min
Estimated Pressure Drop	0.3–1	bar

Table 2.11: Energetic specifications of the traction converter.

2.3.4 Mechanical Specifications of the Traction Converter

The traction converters are designed to be mounted in close proximity to the electric motors to minimize parasitic inductance, reduce cabling complexity, and improve overall thermal management. The mechanical housing ensures high power density and incorporates a direct liquid-cooled PinFin baseplate for effective heat dissipation.

Table 2.12 summarizes the main mechanical specifications of each converter.

Maximum dimensions	$205 \times 123 \times 40\,\mathrm{mm}^3$
Enclosed volume	1.01 L
Mass	0.72 kg
Cooling method	PinFin direct liquid cooling
Protection rating	IP6K9K

Table 2.12: Mechanical specifications of the traction converter.

2.3.5 Sensors in the traction converter

In Tab. 2.13 are listed the types and quantities of sensors integrated within the inverter modules and associated electric drives. These sensors are essential for real-time control, protection, and monitoring.

Measured magnitude	Type	Qty
dc-link voltage	Insulated amplifiers	1
Phase currents (UVW)	Hall effect	3
Inverter temperature	NTC	1
Inverter coolant temperature (IN/OUT)	NTC	2
Motor temperature	NTC	1
Motor coolant temperature (IN/OUT)	NTC	2
Rotor position	Resolver or Encoder	1

Table 2.13: Sensors implemented in the inverter and traction motor.

2.3.6 Control section of the traction converter

The inverter units are operated using a PWM-based control technique with Space Vector Modulation (SVPWM), capable of handling high switching frequencies and optimized torque control in IPM machines. The signals acquired by the control section are: dc-link voltage (V), three-phase currents (I), temperatures (T) of the inverter and motor, and rotor angular position (θ). Tab. 2.14 reports the control unit specifications.

Type of control	SVPWM
Processor	ST SPC58EC80E3 (dual-core) + Resolver to Digital Converter
Analog signals to acquire	V, I, T, θ
Maximum expected consumption	$\sim 50\,\mathrm{W}$
Communication type	CAN-FD
Operating voltage	3.3 V

Table 2.14: Specifications of the control unit for the traction converter.

2.3.7 Specification of the DC/DC Converter

As shown in Tab. 2.15, the DC/DC converter characteristics reported below refer to the target specifications we aim to achieve in this project phase. The selected architecture is intended to provide continuous power delivery to the auxiliary 12 V battery and loads, while ensuring galvanic isolation between the high-voltage traction battery and the low-voltage system.

The preliminary design considers a nominal output power of approximately 6 kW, with an input voltage range compatible with the traction battery (up to 1000 V). The converter should operate reliably under harsh conditions, maintaining an efficiency above 94%.

Continuous output power	$\sim 6\,\mathrm{kW}$
Output voltage (configurable)	0–80 V
Typical output voltage ch1	9-16 V
Input voltage range	Up to 1000 V
Efficiency	>94%
Cooling type	Liquid cooling
Insulation class	Reinforced 4000 VDC
Protection level	IP68/IP6K9K
Max operating temperature	80 °C
Weight	$< 4\,\mathrm{kg}$

Table 2.15: Preliminary target specification of the LV DC/DC converter module.

2.4 Charging system specifications

2.4.1 External charging system

Table 2.16: External charging system.

Connection Type	Combo CCS2 EU	
Charging mode	Mode 4	
Max Power	350	kW
Voltage - Defined by IEC 62196-3	150-920	V
Actual Charging Voltage	650-900	V
Maximum Current	≈ 400	A
Expected Efficiency	90 - 95	%

2.4.2 On board charging system

Table 2.17: On board charging system.

Connection Type	Conductive (Charging Spot)	
Charging mode	Mode 3	
Cooling Type	liquid	–
Power	22	kW
Voltage AC Side (1-phase/ 3-phase)	230/400	V
Voltage DC Side	650-900	V
Current (1-phase/ 3-phase)	$\approx 32/60$	$A(Max.)$
Expected Efficiency	95	%
Max Temperature In	-40	°C
Max Temperature Out	60	°C
Flow Rate	6-10	l/min

2.4.3 Charging time

Table 2.18: Charging time.

Time[min]	Charging type
105	**CCS2 EU - Mode 4**
600	**Conductive - Mode 3**

It should be noted that the power is not considered constant throughout the whole charging procedure. In particular, the considered power has the following scheme:

- SOC from 10 to 30 %: Power equal to the maximum one available from the charging station;
- SOC from 30 to 80 %: Power gradually reduced to half the maximum value to protect the battery;
- SOC from 80 to 100 %: Slow charge to avoid overvoltage;

2.5 Electric Machine

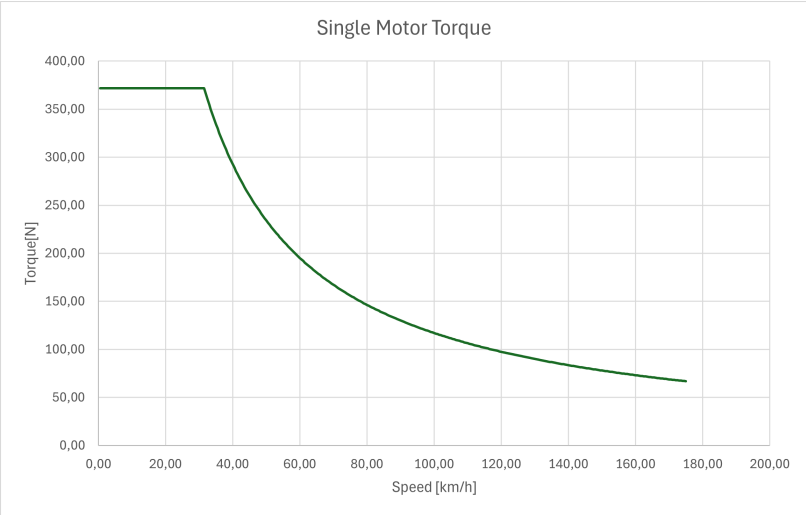

Figure 2.5: Torque vs Speed Motor spec. graph

2.5.1 Electric and Energetic Specifications of the Electric Machine

The traction motor considered for this project is a high-performance Permanent Magnet Synchronous Machine (PMSM), suitable for electric utility vehicles with independent wheel drive. The specifications below reflect the target envelope we aimed to meet.

Motor type	Radial PMSM
Pole pairs	5
Nominal DC voltage	300–450 V
Continuous torque (motor side)	340 Nm
Peak torque (wheel side)	500 Nm
Base speed	5000 rpm
Maximum speed	12000 rpm
Rated power (S1)	175–180 kW
Peak power	275 kW
Efficiency (peak)	>97%
Cooling type	Liquid (50% water – 50% glycol)
Protection class	IP67
Control strategy	Field-oriented control (SVPWM)

Table 2.19: Preliminary electrical and energetic specifications of the traction motor.

2.5.2 Mechanical Specifications of the Electric Machine

The mechanical design fits within our vehicle constraints while ensuring thermal efficiency and robustness. The following specifications represent the indicative values we aimed to meet with the selected motor.

Outer diameter	300–350 mm
Axial length	300–400 mm
Dry mass	79 kg
Rotor inertia	n.a.
Maximum operational speed	12000 rpm
Cooling method	Direct liquid (50/50 mix)
Environmental compliance	IEC standard-based
Protection level	IP67

Table 2.20: Preliminary mechanical specifications of the traction motor.

2.5.3 Sensors for the electric machine

The electric machine requires dedicated sensors for thermal protection and rotor position control. Table 2.21 lists the types and minimum required specifications.

Temperature sensor type	NTC
Min. number of temperature sensors	1
Max allowable sensor temperature	$\geq$180 °C
Rotor position sensor	Resolver

Table 2.21: Sensors required for the electric machine.

2.6 Transmission

Type of transmission	Planetary (2-stage)
Gear ratio	11:1
Input shaft speed (max)	12 000 rpm
Input torque (nominal)	300-350 Nm
Output torque (continuous)	3 500 Nm
Output torque (peak)	4 400 Nm
Output shaft speed (max)	1100 rpm
Efficiency	>96%
Cooling	Oil circulation
Weight	∼50 kg

Table 2.22: Transmission specifications for single-wheel electric drive

2.7 Cooling System

2.7.1 Battery Cooling System

The battery cooling system consist of a single pump that cools down all the modules in series. It is necessary to underline that the Battery Pack and the on-board charger share the same cooling system. The radiator, is positioned in the front of the vehicle to optimize the amount of air that goes through it. The flow rate is calculated as follows:

$$\dot{V} = \frac{Q}{\rho \cdot C_p \cdot \Delta T}$$

If we compute the calculation considering ΔT equal to 25, the value of flow rate is around 17 l/min. The value has been reduced to 15 l/min, this has been done for the following reasons:

- Scaling, corrosion, or long-term degradation of cooling components (clogged channels, reduced pump performance...)
- Avoiding oversize of the pump that would lead to more energy consumption and a cooling system heavier and more expensive;
- Practical systems typically operate at $\approx$ 90% of theoretical flow rates to balance performance and reliability.

Table 2.23: Battery Cooling System

η	92%	
Weight	$860kg$	
Volume	$0.804m^3$	
Cooling Type	liquid	Water and glicole (50-50)
Input temp of cooling liquid	25	$°C$
output temp of cooling liquid	50	$°C$
Worst case ambient temperature	35	$°C$
Flow rate	15	$\frac{l}{min}$
Pressure drop	≈ 1.5	bar
Cooling sequence	Series between modules	
Radiator Weight	6	kg
Radiator Volume	10	l
Consumption on auxiliaries	≈ 500	W
Use of thermal energy	Cabin heating	

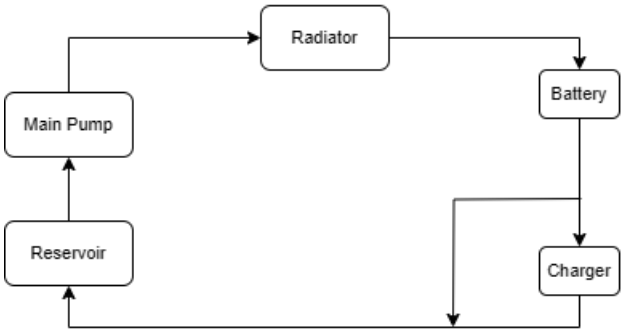

Figure 2.6: Cooling schematic battery and charger

2.7.2 Inverters and motors cooling system

Table 2.24: Cooling system for converters and electric motors

Cooling type	Liquid cooling	50-50 water-glycole
Sequence of Cooling	parallel split post radiator	
Weight	17	kg
Volume	0.03	m^3
Input temp of cooling liquid	40	$°C$
output temp of cooling liquid	70	$°C$
Worst case ambient temperature	50	$°C$
Flow rate	10 (per branch)	$\frac{l}{min}$
Pressure drop	≈ 0.6 per branch	bar
Radiator Weight	8-10	kg
Radiator Volume	9-11	l
Consumption on auxiliaries	≤ 400	W

In the case of the converters and electric motors, the system is again in parallel following the path set by the battery and its charging system (but the two cooling circuits are completely separated between each other). In this case, the two circuits will be identical. One will cool the inverters and motors on the left side and the other one will cool the traction components on the right side. As can be seen in the figure below there are two separate pumps, one per each branch.

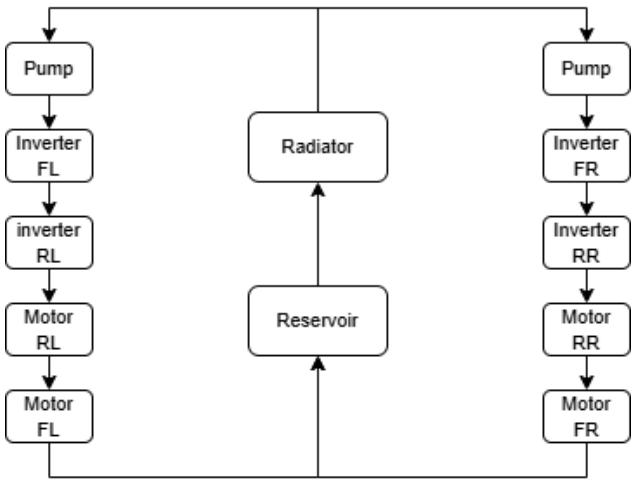

Figure 2.7: Cooling schematic inverter and motors

Chapter 3

Part 3: The Design

3.1 The storage system

Considering the preliminary cell specification that can be found in 3.2, this section is focused on the architecture of the battery pack. Considering the mission, the requirements for the HV accumulator are reported below.

Table 3.1: Accumulator requirements

	Value	**Measurements Unit**
Energy	≈ 200	kWh
Autonomy	**300**	km

The cell taken in consideration during the specifications are the amsung SDI 21700-50E. Some of the cell specifications are reported below.

Table 3.2: Cell Samsung SDI 21700-50E [2]

SDI 21700-50E		
Capacity	4.9	Ah
V_{nom}	3.6	V
Lower Limit Voltage	4.2	V
Upper Limit Voltage	2.5	V
Weight	68.8	g
Tipology	Cylindrical	
Diameter	20.25	mm
Height	70.8	mm
Charge Temperature Range	0 to +45	$°C$
Discharge Temperature Range	-20 to +60	$°C$

Figure 3.1: Samsung SDI 21700-50E

Figure 3.2: Cell weight

Considering the maximum level of voltage set by us at 900 V, the number of cell in series can be found as follows.

$$n_{series} = \frac{900}{4.2} \approx 214$$

Considering the total number of cells (11342), the total number of parallels can be found:

$$n_{parallel} = \frac{11342}{214} = 53$$

Taking into account the calculations, the final configuration of the battery pack is **214s53p**. To allow greater maintainability, modularity and better thermal control, the battery pack is divided into 12 modules, bringing the configuration per each module to **18s53p**. The main characteristics of the battery pack are:

- Each module has a maximum voltage of 75.6 V and a capacity of 317.5 Ah.
- The maximum voltage of the battery pack is 899 V;

To optimize thermal performance and electronic integration:

- Cells are organized in a two-layer structure per module, with temperature sensors placed between the layers to optimize sensor efficiency;
- Positive and negative terminals are located on opposite sides of the module to reduce copper busbar lengths and electrical resistance;
- The BMS is located on top of the upper cell layer to enable cell monitoring and balancing.

The modules, will be placed on the bottom part of the Hilux. Below, a sketch with the Electrical interconnection between the modules in the battery pack is reported.

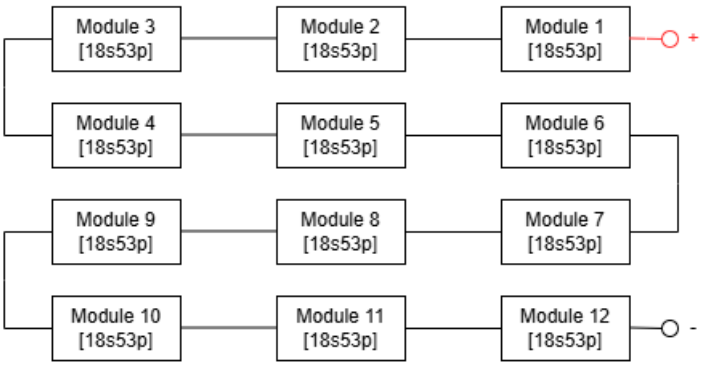

Figure 3.3: Module disposition

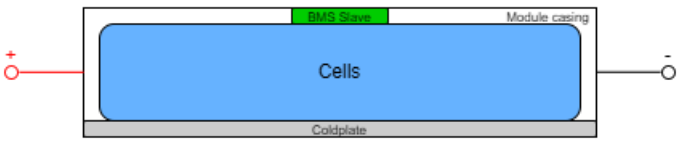

Figure 3.4: Module internal configuration

The module disposition optimizes the weight distribution and consequently the dynamic behaviour of the vehicle. Moreover, this distribution allows for a simplified cooling layout for the battery pack. The principal characteristics of the module are reported below.

Table 3.3: Module characteristics

	Value	Unit Measure
V_{nom}	64.8	V
Lower Limit Voltage	75.6	V
Upper Limit Voltage	45	V
Weight (only cell weight considered)	≈ 65.6	kg
Length	≈ 1100	mm
Width	400	mm
Height	100	mm

Taking into account the table 3.3 and Fig. 3.3, it is possible to verify that the maximum length of the battery pack, equal to $\approx 3.3m$, is below the length of the vehicle that can be found in the table 1.1 (equal to 5.3 m). The same can be done for the width. In this case, the width of the HV accumulator is $\approx 1.2m$, below the internal width of the Hilux equal to 1.54 m (we refer to the distance between the internal part of the tires).

3.1.1 Protection elements

To guarantee a proper power transfer between the High Voltage battery and the inverter, a fuse for dedicated protection and a filtering stage has been introduced. As shown in the figure below, the following elements are included in the DC-link interface:

- **Pre-charge circuit**: composed by a relay and a resistor. It is used to avoid the high inrush currents during the initial closing of the relays. Moreover, it allows a gradual increase in the DC-link capacitor charge;
- **Two main Relays**: one closer to the positive terminal and the other one to the negative one. They allow a controlled connection and disconnection between the battery from the inverter;
- **Fuse**: positioned downstream the battery terminal to provide a fast-acting over-current protection in case of short-circuit faults;
- **LC Filter**: consisting of a series between an inductor L and a parallel capacitor C_{dc}. It is introduced to smooth the voltage ripple and limit the EM interference generated by the inverter. This filter will be analysed and components are going to be designed in the next chapter, the one related to the inverter.

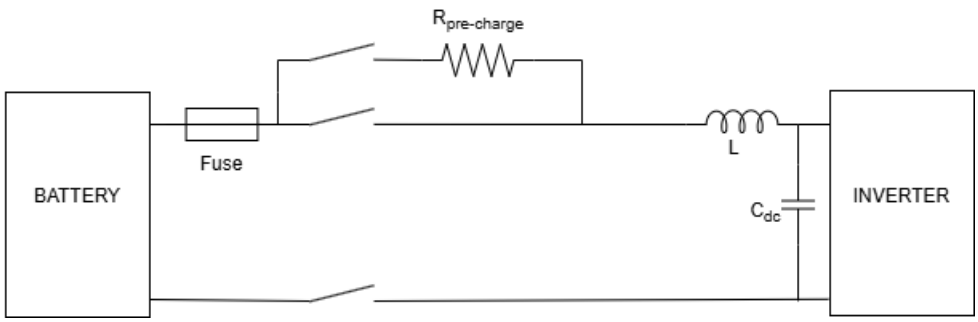

Figure 3.5: Battery pack protection and LC filter schematic

3.1.2 Over-current

The selected fuse for our accumulator is the MDC10M400B manufactured by Mersen. The characteristics of the device are reported below.

Table 3.4: Specification of Mersen MDC10M400B

Parameter	Value
Rated voltage	1000 V
Rated current	400 A
DC Minimum breaking capability	800 A
DC Maximum interrupting capability	65 kA
Melting I_t^2	63 kA^2s
Clearing I_t^2 @1000V DC, L/R = 1 ms	233 kA^2s
Power loss @80% I_n	27 W
Standards	IEC 60269-7; UL E2137 (AC) ; UL E333668 (DC)

Figure 3.6: MDC10M400B - Mersen [3]

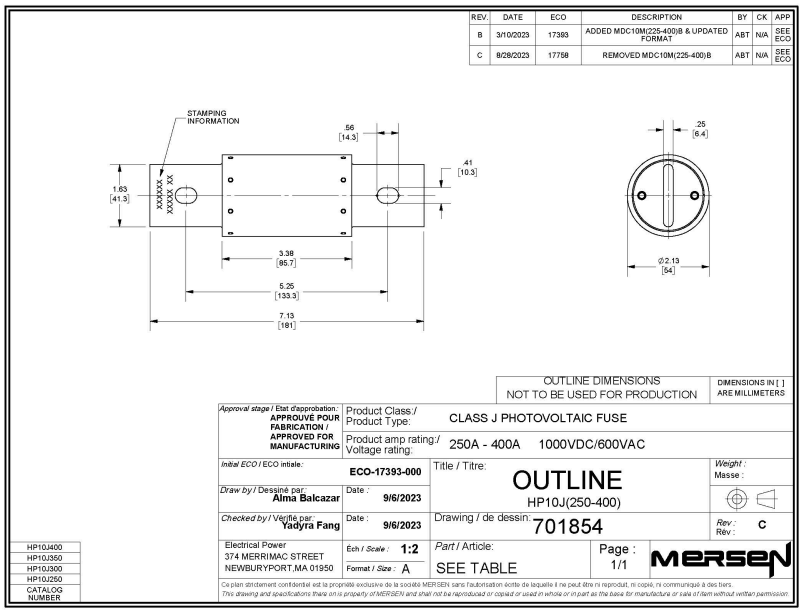

Figure 3.7: Technical draw MDC10M400B - Mersen

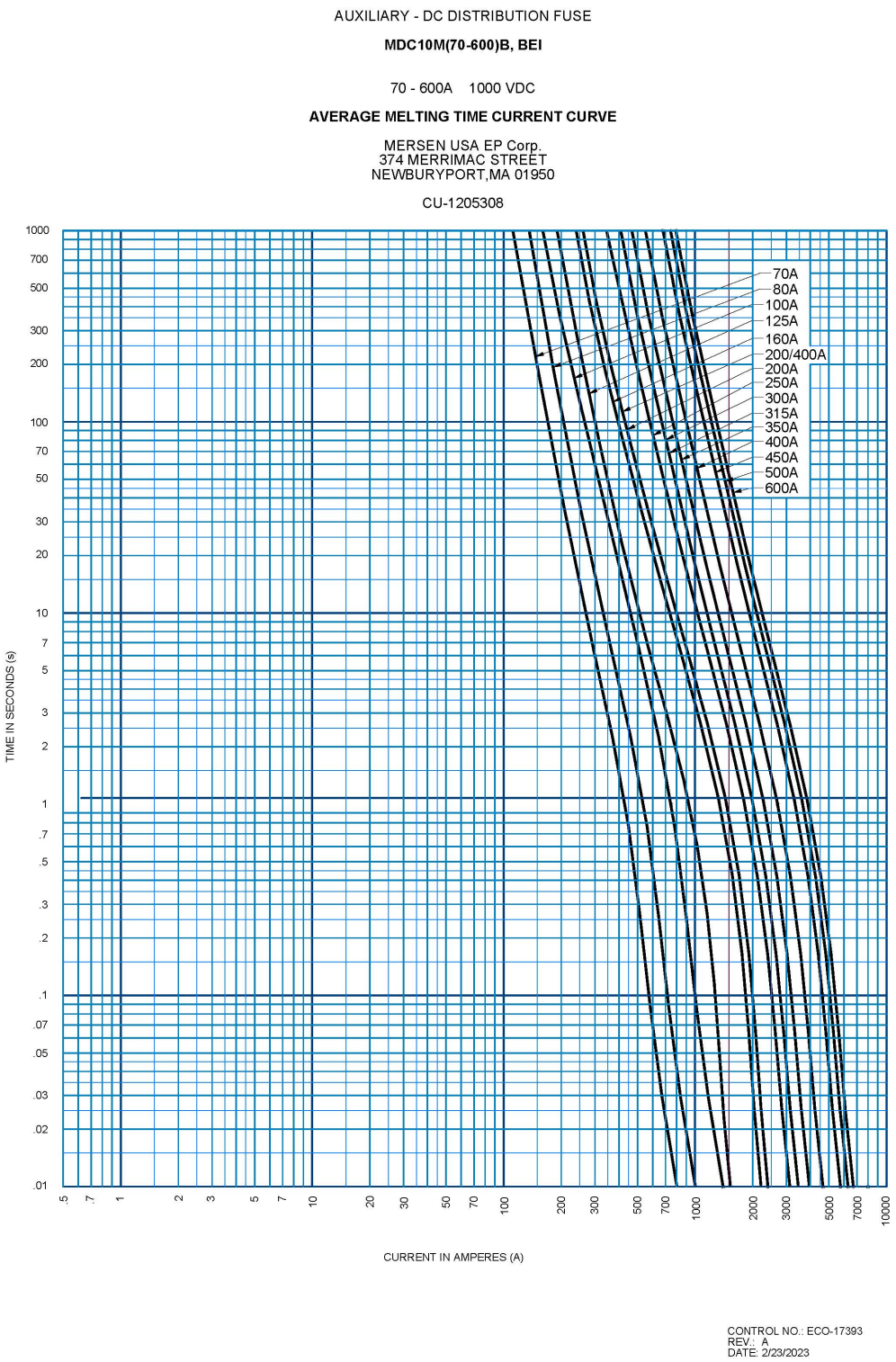

Figure 3.8: Time current curves MDC10M400B - Mersen

An interesting information given by the supplier can be found in the next graph. In particular, we can appreciate the derating of the ampere rating with respect to the temperature. Considering that our accumulator can reach maximum $+60C$, the maximum

derating coefficient achievable stands around ≈ 0.83 which would lead to a nominal current of 373.5 A (still higher than the maximum current achievable in discharge, imposed by us equal to 350 A in the table 2.3.

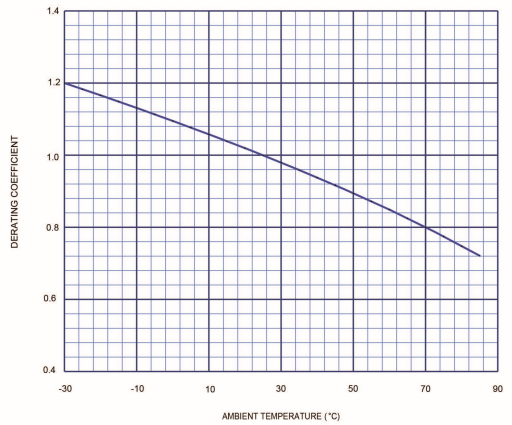

Figure 3.9: Derating curve MDC10M400B - Mersen

3.1.3 Main Relays (AIR) selection

To provide a safe disconnection between the battery pack and the inverters, two high voltage DC contactors are used. The chosen model is the GVB351BAX manufactured by Sensata technologies. In the following, the main characteristics of the chosen model are reported.

Table 3.5: Sensata GVB351BAX specifications

Parameter	Value
Rated voltage	1000 V
Continous current	500 A
Max Brake current	500 A @1000 V DC (1 cycle)
Contact Resistance	0.15 $m\Omega$ (typical)
Mechanical Life	300000 cycles
Coil operating voltage	24 V
Holding Power	2.3 W
Environmental seal	IP67 e IP69K

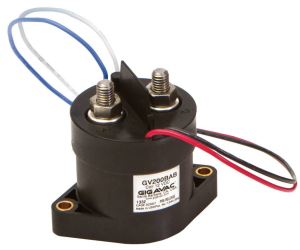

Figure 3.10: Sensata technologies GVB351BAX [4]

3.1.4 High Voltage harness and connectors

Considering our system, both the harness and the connectors need to be able to sustain voltages up to 900 V and peak currents of 540 A. For these reasons, it is necessary to establish stringent requirements for both systems in terms of current capacity, thermal endurance, and insulation level.

High Voltage Harness

To satisfy the requirements listed above, a shielded high voltage cable with a copper conductor with a 150 mm^2 section has been chosen. Below, the main feature are reported:

- XPE insulation rated for voltages up to 110 kV;
- High density polyethylene (HDPE) outer sheath;
- Semiconductive and copper tape shielding for EMI suppression;
- Conductor: Stranded copper, class 2.

Figure 3.11: High voltage single-core cable (150 mm^2)

High Current connector

After the evaluation of the available products, the chosen connector is the one produced by TE connectivity. In particular, considering also the requirements explained in the introduction of this paragraph, the **PowerTube 1400** was chosen. Below, the main characteristics can be found.

Parameter	**Value**	**Unit**
Rated Voltage	1000	V
Rated Current	up to 580	A
Operating Temperature Range	-40 / +150	C
Protection Class	IP6K9K / IP68	–
Cable Compatibility	70–150 mm^2 Cu	–

Table 3.6: Electrical and Mechanical Connector Parameters[5]

Figure 3.12: TE Connectivity PowerTube 1400 high-voltage connector

3.1.5 Sensors

To guarantee a more efficient and safer use of the whole battery pack system, a combination of current, voltage, temperature and insulation sensors are necessary. In particular, their main function is to collect data and are responsible for protection, and real-time communication with the Battery Management System (BMS).

IVT-S Current and Voltage Sensor

The integrated current-voltage sensor selected for this application is the **Isabellenhtte IVT-S**, a high-accuracy transducer optimized for high-voltage DC environments.

The IVT-S module is capable of measuring:

- Bidirectional current up to ±2500 A

- Voltage (U1/U2/U3) up to ±1000 V
- Internal temperature
- Accumulated energy and charge

This sensor integrates galvanic isolation and offers configurable sampling rates, overcurrent protection, and internal diagnostics to improve the safety and reliability of the system.

Figure 3.13: Isabellenhtte IVT-S sensor[6]

IMD - Insulation monitoring device

The insulation monitoring device (IMD) selected is part of the ISOMETER IR155 series produced by Bender. The main characteristics of this device, are reported in the table below.

Parameter	**Value**	**Unit**
Rated Voltage	3500 V / 1 min	V
Rated Current	0 to 1000	A
Measuring Range	0 to 10	$M\Omega$
Supply Voltage	10 to 36	V
Operating Temperature	-40 to +105	C

Table 3.7: Bender Insulation monitoring Device Parameters

Figure 3.14: Bender ISOMETER IR155 sensor[7]

Temperature Sensor

To monitor the temperature within the battery modules, NTCs manufactured by Amphenol are used. These thermistors are distributed strategically, with each module incorporating at least 2 to 3 sensors positioned at thermally critical points:

- On the upper layer of the cells
- Close to busbars or other high-current regions
- At the core of the module

Manufacturer	Amphenol
Model	NK103C4R1
Typology	NTC thermistor

Parameter	**Value**	**Unit**
Resistance @25C	10	kΩ
Operating temperature	-40 to +150	C
Temperature accuracy (0 to 70C)	± 0.2	C
Response time	<15	s
Weight	4	g

Table 3.8: Amphenol NK103C4R1 - Technical data

Figure 3.15: Amphenol NK103C4R1 sensor

3.1.6 BMS - Battery Management System

The battery pack is composed of ≈ 11500 total cells organized into 12 physical modules connected in series. To ensure the safety and monitoring of such complex system, a distributed Battery Management system is required. For the architecture, the chosen one is the Modular/Distributed one. Considering what has been sad up to now, we need one master and at least 12 slaves, one per each module. The chosen BMS is the Orion BMS 3. The expansion units are able to monitor up to 18 cells which perfectly fits the number of cells in series present in our module. Each expansion is able to monitor cell voltages, perform passive balancing and read local temperatures through the NTC thermistors. The master handles the overall SoC, fault handling, charger control and CAN communication with the VCU.

Parameter	**Value**
BMS Architecture	Distributed (Master + CMUs)
Voltage Range	12 1000 V DC
Max Cells in Series	180 (extendable with expansion modules)
Monitored Cells	228 (with 12 18s configuration)
LMUs Required	12 (1 per module, each 18s)
Max Balancing Current	200 mA (passive)
Temperature Range	40 to +85C
Voltage Accuracy	5 mV
Current Measurement	External shunt (user-defined, e.g., 400 mV full scale)
Communications	CAN 2.0B, USB (via CANdapter), RS232 optional
Safety Events Detected	20+ faults: OV, UV, OT, OC, isolation faults, etc.

Table 3.9: Technical specifications of the Orion BMS 3 (Modular) used in the battery pack design.

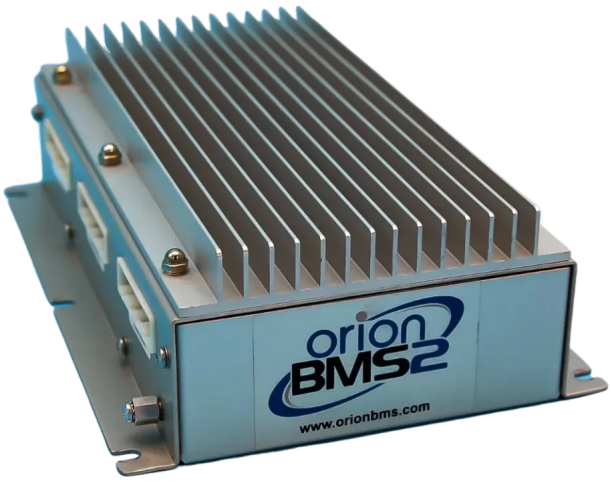

Figure 3.16: Orion BMS 2 Master Unit[8]

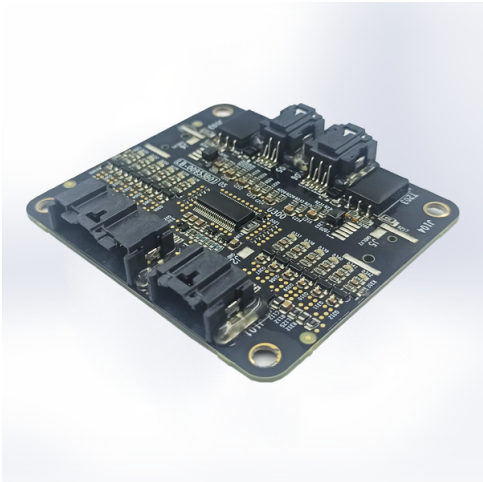

Figure 3.17: Orion BMS Cell Monitoring Unit (CMU)

Below, a schematic which summarize all the main connections of the battery pack system are showed.

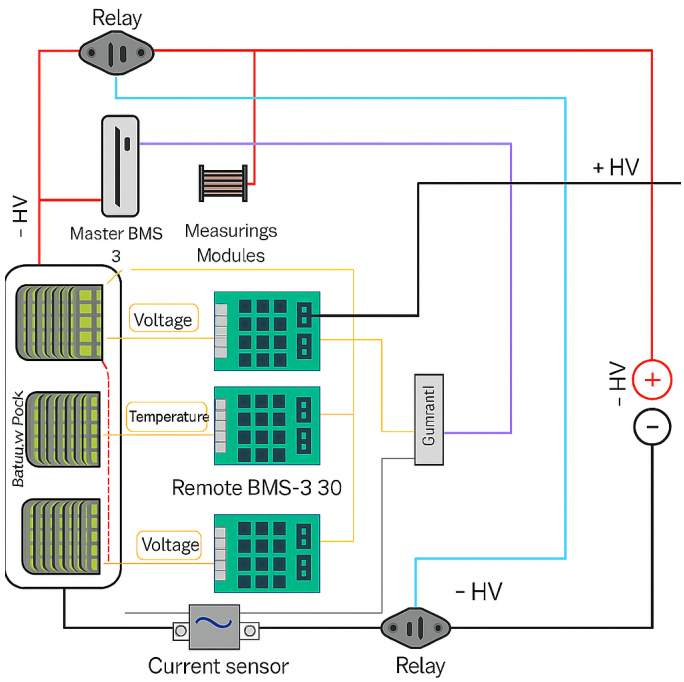

Figure 3.18: Orion BMS schematic

3.1.7 Pre-charge Circuit sizing

To safeguard the inverter and prevent high inrush currents during initial power-up, a pre-charge circuit is used. This circuit slowly charges the DC link capacitors via a current-limiting resistor, preventing potential damage to semiconductor switches and minimizing stress on power contacts.The circuit consists of a resistor in series with a relay, both placed in parallel to the main high-voltage contactor. Considering a capacitance equal to $1000\mu F$ and a desired pre-charge duration of $1s$, the pre-charge resistor can be computed as follows:

$$R_{\text{pre}} = \frac{t_{\text{precharge}}}{5 \cdot C} = \frac{0.5}{5 \cdot 1000 \cdot 10^{-6}} = 100\,\Omega \tag{3.1}$$

$$\tag{3.2}$$

Considering the maximum operating voltage of the Battery pack, and an internal battery resistance of $R_{batt} = 108m\Omega$, we can calculate the in-rush current:

$$I_{\text{pre}} = \frac{V_{\text{batt}}}{R_{\text{batt}} + R_{\text{pre}}} = \frac{900}{0.108 + 100} \approx 8.99\,\text{A} \tag{3.3}$$

$$\tag{3.4}$$

The instantaneous power dissipated by the resistor at t = 0 can be computed as follows:

$$P_{\text{peak}} = R_{\text{pre}} \cdot I_{\text{pre}}^2 = 100 \cdot (8.99)^2 \approx 8.0\,\text{kW} \tag{3.5}$$

Since the inrush current decreases exponentially as the capacitor charges, the average power dissipated by the resistor during the entire pre-charge phase is substantially lower than the initial peak power (typically around 15% to 25% of the peak value). Therefore, the selected resistor must be capable of handling the peak power briefly, while its continuous rating should correspond to the average thermal load generated throughout the pre-charge duration.

The chosen pre-charge relay is the same one used for the main relays, so the **Sensata Technologies GVB351BAX**, rated for 1000 V DC. The resistor used, is the **TE Connectivity HSA50180RJ** which has a nominal value of 180Ω.

Table 3.10: Pre-charge resistor specifications

Manufacturer	TE Connectivity
Model	HSA50180RJ
Resistance	180 Ω
Configuration	Single unit
Dielectric Withstand	3000 V_{DC}
Maximum Temperature	250°C

Figure 3.19: TE Connectivity HSA50180RJ resistor [9]

3.2 Traction Motor

Based on the required performance, the next step is to choose a motor that meets the specifications outlined in Table 3.11. The proposed architecture uses 4 electric motors

placed on every wheel. To determine the suitable motor for the electrification of the vehicle, the target specifications are listed as follows:

Maximum Torque at wheels	$T_{\text{wheel max}} = 13824$ Nm
Maximum Power at wheels	$P_{\text{wheel max}} = 280$ kW
Maximum Speed	$V_{\text{max}} = 175$ km/h
Base Speed	$V_b = 30$ km/h

Table 3.11: Required specifications.

To evaluate whether the selected motor meets these requirements, the speeds are converted to RPM:

$$n_{\text{max}} = \frac{175 \cdot 1000}{2\pi \cdot 0.432} \cdot \frac{1}{60} = 1074.84\,\text{rpm}$$

$$n_b = \frac{v_{\text{base}}}{2\pi r} \cdot \frac{1000}{60} = \frac{30}{2\pi \cdot 0.432} \cdot \frac{1000}{60} \approx 184\,\text{rpm}$$

Given the performance requirements, the BRUSA HSM2-10.18.22 motor is selected for evaluation. Its main technical features are reported in Table 3.12.

Manufacturer	BRUSA
Model	HSM2-10.18.22
Maximum Speed n_{max}	12000 rpm
Nominal Speed n_{nom}	5000 rpm
Continuous Torque T_{cont}	340 Nm
Maximum Torque T_{max}	500 Nm
Continuous Power P_{cont}	175 kW
Maximum Power P_{max}	275 kW
Efficiency (typ.)	97.5%
Pole Pairs	5
Number of turns	6
Voltage V_{alim}	300–450 V
Insulation class	H
Nominal Frequency	417 Hz
Maximum Frequency	1000 Hz
Power factor $\cos(\phi)$	0.95
Weight (without gearbox)	79 kg
Volume	23.3 l
IP Protection	IP67
Coolant inlet temp. (min)	-30 C
Coolant outlet temp. (max)	65 C
Coolant flow rate	6–10 l/min
Pressure drop @ 8 l/min	0.26 bar

Table 3.12: Specifications of the BRUSA HSM2-10.18.22 electric motor [10].

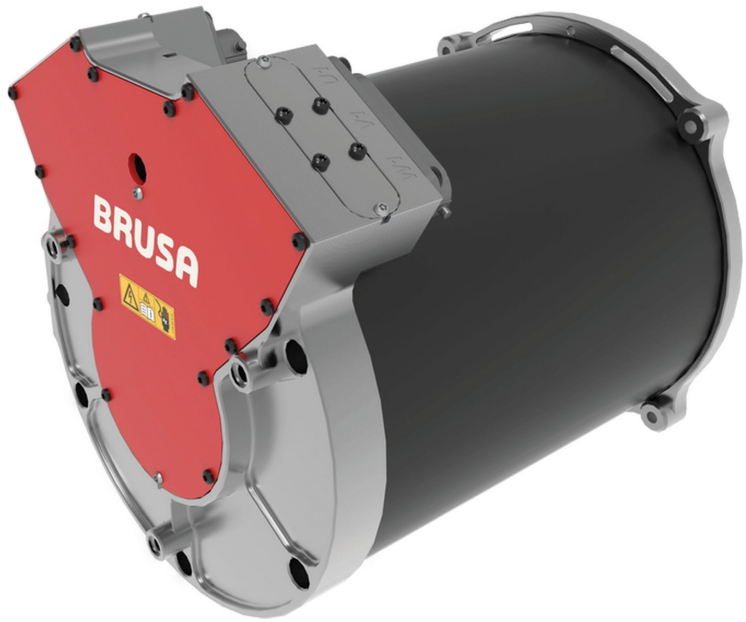

Figure 3.20: QBrusa Motor HSM2-10.18.22

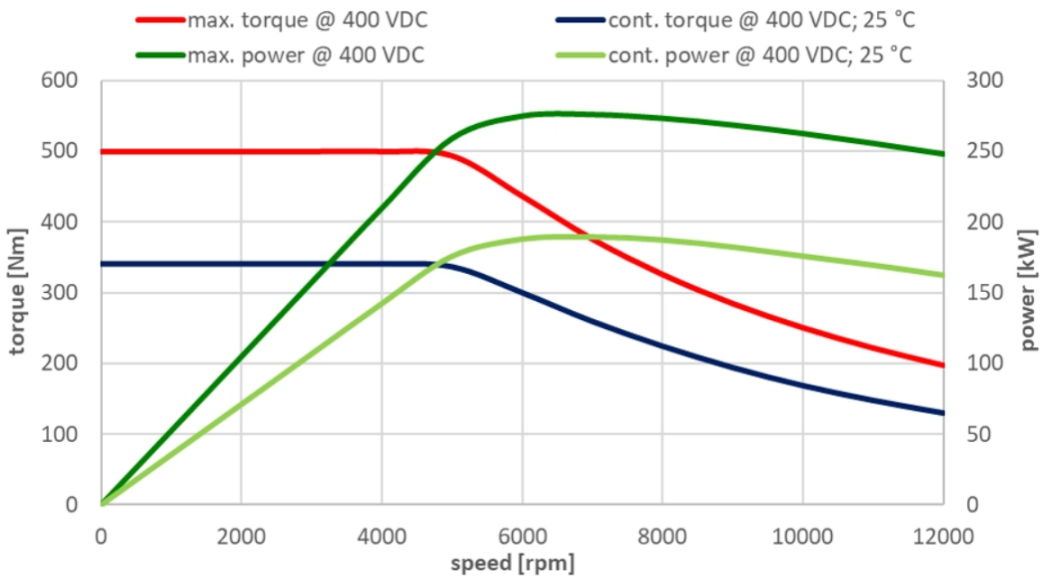

Figure 3.21: Torque - Speed characteristc

To meet the desired output continuous torque at the wheels, we first try a gear ratio of 11:1 and assume an efficiency of $\eta_g = 0.94$:

$$T_{\text{wheel}} = T_{\text{max}} \cdot r_g \cdot \eta_g = 340 \cdot 11 \cdot 0.94 = 3515\,\text{Nm}$$

$$P_{\text{motor max}} = \frac{P_{\text{wheel max}}}{4 \cdot \eta_g} = \frac{280}{4 \cdot 0.94} \approx 74.5\,\text{kW}$$

However, considering 4 motors:

$$T_{\text{transmitted}} = 4 \cdot T_{\text{wheel}} = 4 \cdot 3515 = 14060\,\text{Nm} > 13826\,\text{Nm}$$

$$n_{\text{motormax}} = \frac{n_{\max}}{r_g} = \frac{12000}{11} = 1091\,\text{rpm} > 1074\,\text{rpm}$$

Thus, the torque requirement is met and the rotational speed is acceptable. We now recalculate the base speed at the motor side:

$$n_b' = n_b \cdot r_g = 184 \cdot 11 = 2024\,\text{rpm}$$

$$f_b' = \frac{n_b'}{60} \cdot p = \frac{2024}{60} \cdot 5 = 168.7\,\text{Hz}$$

This confirms that the new operating point, considering the updated gear ratio, is compatible with the motor specifications.

Losses

By referring to the datasheet supplied by the manufacturer, it is possible to estimate the motor's average efficiency by evaluating the relevant operating conditions.

HSM2-10.18.22-B01 efficiency @ 400 V_{DC} (measured with DTI844-6-B01)											
Torque [Nm]											
500	91.6	95.1	96.2	96.7							
480	91.8	95.2	96.3	96.8	97.1						
460	92.0	95.3	96.4	96.9	97.1						
440	92.3	95.4	96.5	97.0	97.2						
420	92.6	95.6	96.6	97.0	97.2	97.1					
400	92.8	95.8	96.7	97.1	97.3	97.2					
380	93.1	95.9	96.8	97.2	97.4	97.3					
360	93.4	96.0	96.9	97.2	97.4	97.4	96.9				
340	93.6	96.2	97.0	97.3	97.4	97.5	97.1				
320	93.9	96.3	97.0	97.4	97.5	97.5	97.2				
300	94.1	96.4	97.1	97.4	97.5	97.6	97.3	96.7			
280	94.4	96.6	97.2	97.4	97.5	97.6	97.4	97.0			
260	94.6	96.7	97.3	97.5	97.6	97.6	97.5	97.1	96.4		
240	94.9	96.8	97.3	97.5	97.6	97.5	97.5	97.2	96.6		
220	95.1	96.9	97.4	97.5	97.5	97.5	97.5	97.3	96.9	96.3	
200	95.3	97.0	97.4	97.6	97.5	97.4	97.5	97.3	97.1	96.5	95.7
180	95.6	97.1	97.4	97.5	97.5	97.4	97.5	97.4	97.1	96.8	96.2
160	95.8	97.1	97.5	97.5	97.4	97.3	97.4	97.4	97.2	96.8	96.4
140	95.9	97.1	97.4	97.5	97.4	97.2	97.2	97.3	97.1	96.9	96.6
120	96.0	97.0	97.3	97.3	97.1	96.9	96.8	97.0	97.0	96.8	96.6
100	96.0	96.9	97.1	97.1	96.9	96.7	96.4	96.6	96.7	96.7	96.5
80	96.1	96.9	97.0	96.8	96.7	96.4	96.1	96.1	96.2	96.2	96.2
60	95.9	96.5	96.6	96.4	96.3	95.9	95.5	95.2	95.4	95.4	95.4
40	95.4	95.9	95.8	95.7	95.4	94.9	94.4	94.1	93.7	93.9	94.0
20	93.2	93.3	93.2	93.0	92.6	91.9	91.5	91.2	90.3	89.6	90.0
Q1	1000	2000	3000	4000	5000	6000	7000	8000	9000	10000	11000
	Speed [rpm]										

Figure 3.22: Motors Efficiency.

As observed in Figure 3.22, the motor shows an average efficiency of approximately $\eta_m \approx 94\%$. Assuming this value, and considering that the motor must deliver a peak power of $P_{\text{motormax}} = 74.5\,\text{kW}$, we can estimate the total power losses.

$$P_{\text{losses}} = P_{\text{motormax}} \cdot (1 - \eta_m) = 74.5 \cdot (1 - 0.94) = 4.47\,\text{kW}$$

3.2.1 External Dimensions

This section presents the dimensions occupied by the motor. These are the actual dimensions that will be used, as the chosen transmission ratio eliminates the need for similarity-based modifications to improve the electric machines specifications.

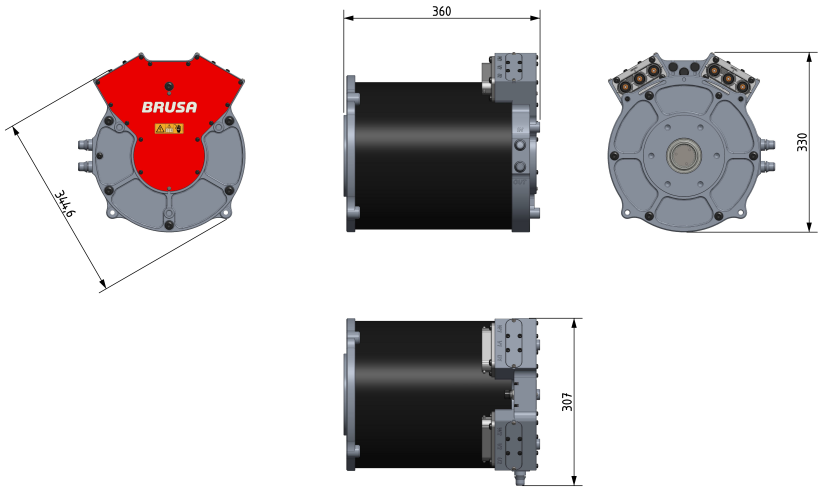

Figure 3.23: Motor dimension.

	Value	Unit
Width	307	mm
Height	330	mm
Length	360	mm
Active Length	220	mm
Rotor Diameter	215	mm

Table 3.13: Main Dimensions for the Electric Machine

3.2.2 Sensor

In order to guarantee accurate motor control and avoid permanent damage to its active components, it is essential to equip the motor with both temperature and position sensors. Conversely, current sensors are not included at this stage, as they are already integrated within the inverter responsible for motor management.

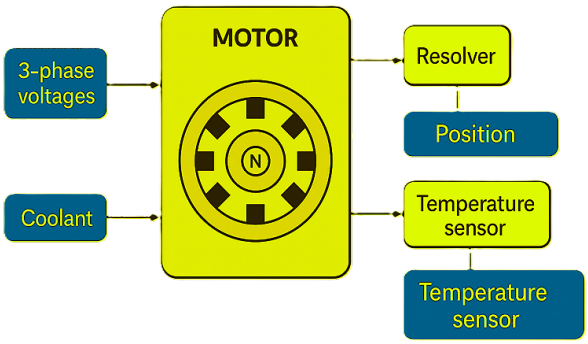

Figure 3.24: Motors input/output.

Temperature sensor

According to standard practices for high-performance permanent magnet synchronous motors (PMSMs) and information from comparable models, it is likely that the motor is equipped with at least two temperature sensors for each phase:

-one monitoring the stator temperature

-and another measuring the coolant temperature

Position sensor

To supply the stator with the correct voltage sequence, the rotor position must be known. To achieve this, the motor uses an analog resolver that provides sine and cosine signals.

Figure 3.25: Motors resolver [11]

Producer	TAMAGAWA SEIKI
Model	TS2605N1E64
Type	1X-BRX
Primary	R1-R2 (Rotor)
Input Voltage	AC 7 Vrms 10 kHz
Transformation Ratio [K]	0.5 5%
Electrical Error	10′
Phase Shift	+10 Nom
Input Impedance	140 Ω
Output Impedance	120 Ω
Allowable Rotation Speed	40,000 rpm
Operating Temperature	−55°C to +155°C
Mass	0.03 kg

Table 3.14: Resolver TS2605N1E64 Specification

3.2.3 Transmission

This section describes the main characteristics of the transmission system chosen for the electrification of the vehicle. A **Double Offset Traction Drive (DTDO)** gearbox has been selected due to its compact design, high torque transfer capabilities, low acoustic emissions, and high overall efficiency. These features make it particularly suitable for heavy-duty electric vehicles with dual-motor configurations.

The selected transmission integrates two high-speed electric machines, each delivering up to 74.5 kW of continuous input power and 340 N m of torque. Thanks to the embedded gear ratio of 1:11, the output torque is significantly increased up to 3515 N m per motor, while the output speed is reduced accordingly to ensure compatibility with the vehicles dynamic requirements.

The DTDO system provides a high efficiency of 94 %, corresponding to an estimated continuous power loss of 16 kW under nominal conditions. The cooling system is based on a hybrid *water + oil* solution, supporting thermal stability during prolonged operation.

Additional benefits include the integration of a differential gear within the same housing, a total system weight of 40 kg, and a compact volume of approximately 40 L.

Table 3.15: DTDO Transmission Main Technical Specifications

Parameter	**Value**
Number of motors	4
Input power (continuous)	4×74.5 kW
Output power (continuous)	4×70 kW
Input torque	4×340 N m
Output torque	4×3515 N m
Input speed	12 000 rpm
Output speed	1091 rpm
Gear ratio	1:11
Efficiency	94 %
Losses	16 kW
Cooling type	Water + Oil
Weight	40 kg
Volume	40 L
Differential gear	Included

3.2.4 Connectors and Cables

To connect the motor to the inverter, two types of conductors are required:

- Power cables.
- Signal cables.

Power Cables For high-voltage three-phase power transmission between the inverter and the motor, we selected a shielded high-voltage cable from Renhotec EV, specifically designed for energy storage and traction systems.

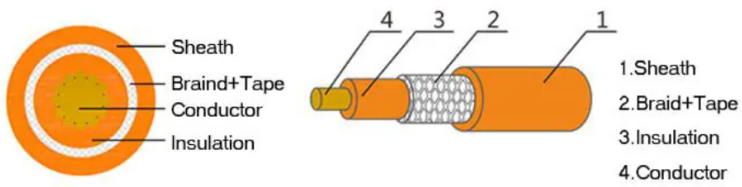

P/N NO.	SIZE	20°C MAXIMUM CONDUCTOR RESISTANCE	RATED VOLTAGE	20°C LOAD ACCEPTANCE CURRENT
EVRP-2.5mm²	2.5mm²	7.6	1.5kV	30A
EVRP-4mm²	4mm²	4.71	1.5kV	40a
EVRP-6mm²	6mm²	3.14	1.5kV	52A
EVRP-10mm²	10mm²	1.82	1.5kV	75A
EVRP-16mm²	16mm²	1.16	1.5kV	100A
EVRP-25mm²	25mm²	0.743	1.5kV	125A
EVRP-35mm²	35mm²	0.527	1.5kV	165A
EVRP-50mm²	50mm²	0.368	1.5kV	215A
EVRP-70mm²	70mm²	0.259	1.5kV	260A
EVRP-95mm²	95mm²	0.196	1.5kV	320A
EVRP-120mm²	120mm²	0.153	1.5kV	370A
EVRP-150mm²	150mm²	0.129	1.5kV	430A

Figure 3.26: Renhotec 150 mm^2 High Voltage Power Cable [12].

The selected cable offers the following specifications:

- Rated voltage: **1500 V DC**
- Continuous current capacity: **430 A**
- Cross-section: **150 mm^2**
- Shielded: Yes (EMC compliant)
- Insulation: XLPE with orange outer jacket, compliant with EV standards
- Temperature rating: **-40 C to +125 C**

This cable meets the current requirement of 400 A per phase while offering additional margin and high thermal and mechanical robustness, making it suitable for the traction environment.

Code	Part number	Cable structure	Conductor material / shield type	Diameter over shield nom.	Outer cable diameter nom.	Insulation material		Jacket material	Service temperature	Impedance	Weight
				[mm]	[mm]	1	2		[°C]	[Ω]	[kg/km]
LVDS											
LEONI Dacar 501	76981008A	4x2x0.22+0.22	Cu bare / PETP-AL / C-shield	5.80	6.80	PE	–	PVC	–40 up to +90	100	56.0
LEONI Dacar 502	76981009A	4x2x0.22+0.22	Cu bare / PETP-AL / C-shield	5.80	6.80	PP	–	PVC	–40 up to +105	100	55.0
LEONI Dacar 503	76981003A	4x2x0.22	Cu bare / PETP-AL / C-shield	5.60	6.80	cellular PP	–	PVC	–40 up to +105	100	56.0
LEONI Dacar 505	76981000A	4x2x0.22+(0.22)	Cu bare / AL coated foil / C-shield	5.50	6.30	PE	–	TPE-U	–40 up to +90	100	51.0
LEONI Dacar 506	76981020A	4x2x0.22+(0.22)	Cu tinned / AL coated foil / C-shield	5.50	6.30	FEP	–	TPE-U	–40 up to +110	100	61.0
LEONI Dacar 508	76981006A	5x2x0.22	Cu bare / PETP-AL / C-shield	6.50	7.40	PE	–	PVC	–40 up to +90	100	63.5
LEONI Dacar 509	76981007A	5x2x0.22	Cu bare / PETP-AL / C-shield	6.00	7.40	PP	–	PVC	–40 up to +105	100	71.0
LEONI Dacar 511	76981060A	5x2x0.22	Cu bare / PETP-AL / C-shield	6.00	7.00	cellular PP	–	PVC	–40 up to +105	100	69.0
LEONI Dacar 522	76981035A	2x0.14	Cu tinned / PVC-AL / C-shield	3.10	4.60	PP	–	PVC	–40 up to +105	100	27.0
LEONI Dacar 538	76981056A	4x0.14	Cu tinned / PVC-AL / C-shield	3.40	4.60	PP	–	PVC	–40 up to +105	100	34.0
CAN											
LEONI Dacar 520	79116800A	2x0.35	Cu bare / PETP	–	4.90	cellular PP	–	TPE-U	–40 up to +105	120	22.0
LEONI Dacar 560	76731000A	2x0.35	Cu bare	–	5.00	TPE-O-X	–	TPE-U	–40 up to +125	120	28.5
LEONI Dacar 562	76731010A	2x0.5	Cu bare / PETP	–	5.40	TPE-O-X	–	TPE-U	–40 up to +120	120	31.0
LEONI Dacar 565	76981030A	2x0.75+(0.75)	Cu bare / PETP-AL	–	8.00	cellular PP	–	PVC	–40 up to +105	120	62.0

Figure 3.27: Dacar 560 series [13]

Signal Cables To connect sensors and low-voltage devices inside the motorsuch as temperature sensors and the resolverto the inverter, shielded multi-core data and signal cables are required. In this project, LEONI Dacar® 560 cables were selected. These cables are specifically designed for automotive signal transmission, offering excellent electromagnetic compatibility (EMC), thermal stability, and mechanical robustness.

The Dacar 560 series is suitable for high-reliability environments and meets international automotive standards such as ISO 6722 and LV 112. The cables are constructed with high-performance copper conductors, thermoplastic insulation, and a dense shielding structure to minimize signal interference. For environmental protection and mechanical connection, the cables are terminated with IP67-rated multipole connectors, ensuring secure operation in high-vibration vehicular contexts.

3.3 Power Electronics

The vehicle's powertrain architecture features seven different power converters, in particular we are using four inverters, two DC/DC converters and one AC/DC converter.

- **Four DC/AC converters (traction inverters)** convert the batterys DC voltage into 450 Vac three-phase power for the electric motors.
- **One DC/DC HV-LV converter** provides 12Vdc power for the vehicles lowvoltage auxiliary systems (Aux LV), such as control electronics and lighting.
- **One AC/DC converter**, also called the on Board Charger. It is used to charge the vehicle during Mode 3 Charging.
- **One DC/DC HV-HV converter** allows the voltages level match between the on board charger and the battery.

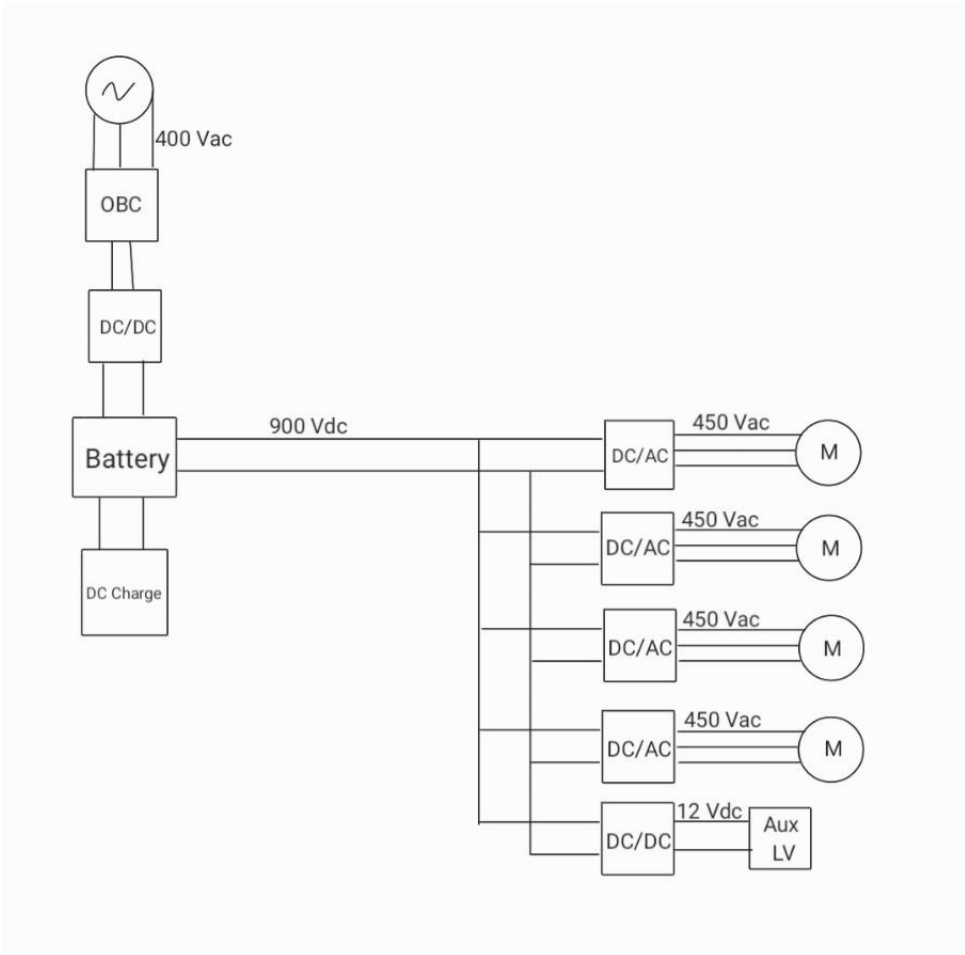

Figure 3.28: Powertrain Schematic

3.3.1 Inverters

The vehicles traction system is powered by four DC/AC inverters that incorporate the **Infineon HybridPACK™ Drive FS03MR12A6MA1LB** module. This module is a robust, automotive-qualified power solution featuring silicon carbide (SiC) MOSFET technology.

Specifically engineered for e-mobility applications, the inverter supports high-voltage operation (up to 1200 V) and delivers continuous high currents, making it a suitable choice for electric vehicle propulsion systems. The table below summarizes the primary specifications of the selected module.

Although the nominal battery voltage is 900 V, the adoption of a SiC inverter rated at 1200 V offers several performance benefits:

- **Reduced switching and conduction losses**, enabled by the intrinsic properties of SiC devices;
- **Higher overall energy efficiency** throughout the drive cycle;
- **Lower thermal management needs**, permitting a more compact and simplified cooling system;

Table 3.15: Main specifications of FS03MR12A6MA1LB module [14].

Symbol	Parameter	Value
V_{DSSmax}	Drain–Source Voltage	1200 V
I_{DS}	Continuous Drain Current	400 A
I_{SBDD}	Body Diode Continuous Current	210 A
$I_{\mathrm{DS(pulsed)}}$	Pulsed Drain Current	800 A
$V_{\mathrm{(BR)DSS}}$	Breakdown Voltage	1200 V
T_{MIN}	Minimum Operating Temperature	$-40\,^{\circ}\mathrm{C}$
T_{MAX}	Maximum Operating Temperature	$150\,^{\circ}\mathrm{C}$
$f_{\mathrm{switching}}$	Switching Frequency	20 kHz

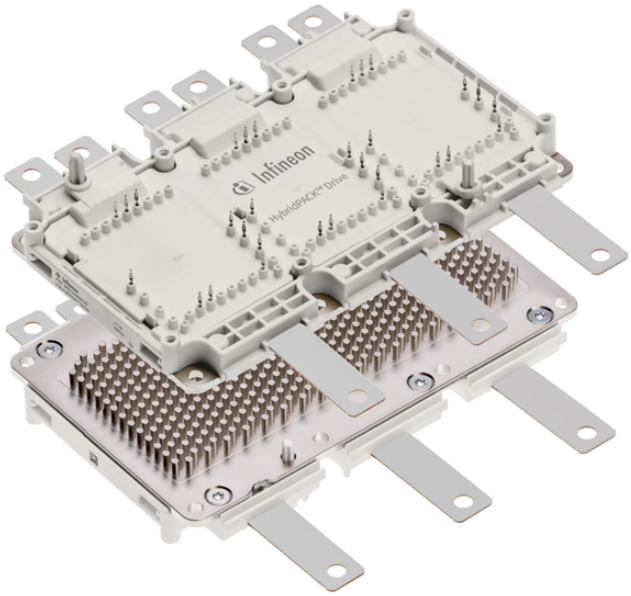

Figure 3.26: Infineon FS03MR12A6MA1LB HybridPACK™ Drive module.

- **Increased reliability**, due to operation with wide safety margins in voltage and current;
- **Alignment with automotive standards**, thanks to features like integrated NTC sensors and durable packaging.

Thanks to SiC technology and direct liquid cooling, the inverter supports high thermal performance and minimal switching losses. The module integrates a PinFin baseplate and is suited for high-efficiency drive systems in electric vehicles.

Parameter	Value
Turn-on energy loss (E_{on})	19.5–20.2 mJ @ 400 A, 600 V
Turn-off energy loss (E_{off})	17.6–18.2 mJ @ 400 A, 600 V
Reverse recovery energy (E_{rec})	1.4–4.7 mJ
Thermal resistance junction-to-fluid	0.10–0.108 K/W
Cooling type	Liquid (50/50 water-glycol), PinFin baseplate
Cooling pressure drop (@10 L/min)	≈640 mbar
Operating temperature range	–40°C to 150°C

Table 3.16: Thermal and energetic characteristics of the SiC traction inverter.

3.3.2 Design of LC Filter between Battery and Inverter

The LC filter installed between the battery pack and the inverter helps suppress voltage and current fluctuations caused by inverter switching. Minimizing these ripples contributes to extending battery life, increasing overall efficiency, and reducing electromagnetic interference (EMI).

The main design parameters are defined as:

$$Z_L = \frac{V_{\text{dc}}^2}{P_{\text{rated}}} \quad \text{(inverter characteristic impedance)}, \qquad f_c = \frac{f_{\text{sw}}}{4} \quad \text{(cut-off frequency)}$$

Where:

- $V_{\text{dc}} = 900\,\text{V}$: nominal DC-link voltage,
- $P_{\text{rated}} = 80\,\text{kW}$: rated output power of the inverter,
- $f_{\text{sw}} = 30\,\text{kHz}$: switching frequency,
- $f_c = 7500\,\text{Hz}$: desired cut-off frequency.

From these, the inverter characteristic impedance is:

$$Z_L = \frac{(900)^2}{80 \cdot 10^3} = 10\,\Omega$$

The LC filter components can then be computed as:

$$L = \frac{Z_L}{2\pi \cdot f_c} = \frac{10}{2\pi \cdot 7500} \simeq 212.2\,\mu\text{H}$$

$$C = \frac{1}{Z_L \cdot 2\pi \cdot f_c} = \frac{1}{10 \cdot 2\pi \cdot 7500} \simeq 2.12\,\mu\text{F}$$

This resonance lies well below the switching frequency of 30 kHz, ensuring stability and effective filtering under full-load operation.

Practical Choice for Real Components

Although the theoretical design yields, such an inductance value may be physically bulky and unsuitable for high-current applications.

To improve feasibility while keeping the cutoff frequency approximately constant, the inductance is deliberately decreased and the capacitance increased. This preserves the filter's behavior while using more compact and readily available components.

Selected practical values:

- $L = 20\,\mu\text{H}$
- $C = 25\,\mu\text{F}$

Verification of the revised cutoff frequency:

$$f_t = \frac{1}{2\pi\sqrt{LC}} = \frac{1}{2\pi\sqrt{20 \cdot 10^{-6} \cdot 25 \cdot 10^{-6}}} \approx 7.12\,\text{kHz}$$

This confirms that the modified LC pair still achieves a cutoff frequency in the same order of magnitude, validating the proposed practical component selection.

- **Capacitors:** 10 C4AQOLU4250P12J in parallel $\rightarrow$ $25\,\mu\text{F}$ total, rated for over **103 ARMS**

Figure 3.29: C4AQOLU4250P12J Metallized Polypropylene Film Capacitor

Table 3.17: Specifications of Capacitor C4AQOLU4250P12J [15]

Parameter	**Value**
Capacitance	$2.5\,\mu\text{F}$
Rated Voltage	900 VAC
Max RMS Current (85C, 10kHz)	10.3 A
Peak Current	220 A
ESR (typical @10kHz)	$4.5\,\text{m}\Omega$
ESL (typical)	18 nH
Operating Temperature	-40C to +105C
Dimensions (WxHxT)	573057 mm
Dielectric	Metallized Polypropylene Film

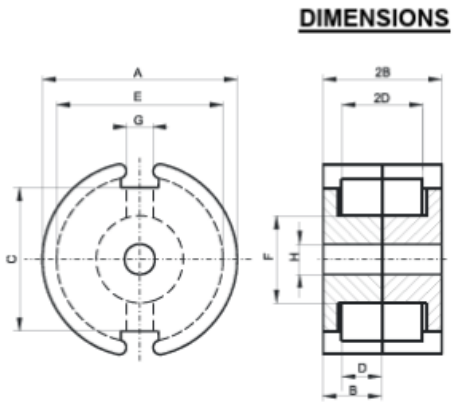

(mm)	Nominal:	Tol. min.:	Tol. max.:
A	25.5	-0.5	+ 0.5
B	8.05	-0.1	+ 0.1
2B	16.1	-0.2	+ 0.2
C	18.0	-0.4	+ 0.4
D	5.5 Min.		
2D	11.0 Min.		
E	21.6	-0.4	+ 0.4
F	11.3	-0.2	+ 0.2
G	3.8	-0.6	+ 0.6
H	5.5	-0.1	+ 0.1
Eff. Parameters			
Ae mm 2	Amin mm 2	le mm	Ve mm 3
93.9	77.4	37.6	3530

Inductor 0W42616UG

Table 3.18: Specifications of Inductor 0W42616UG [16]

Parameter	**Value**
Core Type	Toroidal (Ring Core)
Material	W-type Magnetic Alloy
Dimensions	25.5 21.6 16.1 mm
Effective Core Area (A_{Fe})	93.9 mm^2
Minimum Core Area (A_{min})	77.4 mm^2
Magnetic Path Length (l_{e})	37.6 mm
Effective Volume (V_{e})	3530 mm^3
A_L Value (10 kHz, 25C)	20000 nH (nom.), 14000 nH (min.)
Loss Factor @ 10 kHz	<3.5 (for $B < 0.25$ mT)
Loss Factor @ 100 kHz	< 50 (for $B < 0.25$ mT)
Mounting	Through-hole (no marking, resin encapsulated)

3.3.3 Inverter Losses

The updated peak current is now assumed to be:

$$\hat{I} = 200 \cdot \sqrt{2} \approx 283\,\text{A}$$

Conduction Losses:

$$P_{\text{cond},3\phi/VSI} = 3 \cdot \left[\frac{1}{2} \cdot R_{ds,eq} \cdot \hat{I}^2\right] = 3 \cdot \frac{1}{2} \cdot 0.004 \cdot (283)^2 \approx 480\,\text{W} \tag{3.6}$$

Commutation Losses:
We keep: - $V_{\text{dc-link}} = 900\,\text{V}$ - $\Delta t_{\text{comm}} = 300\,\text{ns} = 3 \cdot 10^{-7}\,\text{s}$ - $f_{\text{sw}} = 10\,\text{kHz}$

$$P_{\text{comm},PWM} = 3 \cdot \frac{2}{\pi} \cdot \hat{I} \cdot V_{\text{dc-link}} \cdot \Delta t_{\text{comm}} \cdot f_{\text{sw}} \tag{3.7}$$

$$P_{\text{comm},PWM} \approx 3 \cdot \frac{2}{\pi} \cdot 283 \cdot 900 \cdot 3 \cdot 10^{-7} \cdot 10^4 \approx 1460\,\text{W}$$

Total inverter losses per unit:

$$P_{\text{loss,tot}} = 480 + 1460 = 1940\,\text{W}$$

For the entire vehicle (4 inverters):

$$P_{\text{loss,tot,4inv}} = 4 \cdot 1940 = 7\,760\,\text{W}$$

Assuming total delivered mechanical power remains:

$$P_{\text{mech}} = 4 \cdot 80\,\text{kW} = 320\,\text{kW}$$

$$\eta_{\text{total}} = \frac{P_{\text{mech}}}{P_{\text{mech}} + P_{\text{loss,tot,4inv}}} = \frac{320}{320 + 7.76} \approx 0.976 \tag{3.8}$$

3.3.4 Capacitor choice

A capacitor must be placed at the inverters input for several key reasons:

- **Filter input current:** It smooths the battery-sourced current entering the inverter, preventing unwanted ripple inside the converter.
- **Suppress harmonics and EMI:** By damping high-frequency components, it cuts down harmonics and the electromagnetic interference they generate.
- **Improve overall efficiency:** Reduced ripple, steadier voltage and lower EMI collectively raise the systems efficiency.

Because both traction inverters drive the same electric motor, the capacitor bank will be sized for a single inverter and can then be duplicated for the other.

We now begin by considering the motors peak current:

$$P_{\text{inv,out}} = \frac{P_{\text{motor}}}{\eta_m} = \frac{74.5}{0.97} \approx 76.8\,\text{kW}$$

$$I_{\text{inv,out}} = \frac{P_{\text{inv,out}}}{\sqrt{3} \cdot V_{\text{ph,inv}} \cdot \cos\varphi} = \frac{76800}{\sqrt{3} \cdot 450 \cdot 0.9} \approx 109.5\,\text{A}_{\text{rms}}$$

$$I_{\text{out,pk}} = \sqrt{2} \cdot I_{\text{inv,out}} \approx \sqrt{2} \cdot 109.5 \approx 154.86\,\text{A}_{\text{pk}}$$

Now, using the following equation, we can calculate the RMS current flowing through the capacitor:

$$V_{\text{ph–ph,max}} = V_{\text{op,max}} \cdot 0.97 = 900 \cdot 0.97 = 873\,\text{V}$$

$$I_{\text{rms,cond}} = I_{\text{out,pk}} \cdot \sqrt{\frac{V_{\text{ph–ph}}}{V_{\text{op,max}}} \cdot \left(\frac{1}{2\pi} + \left(\frac{2}{\pi} - \frac{3V_{\text{ph–ph}}}{4V_{\text{op,max}}}\right) \cdot \cos^2\varphi\right)}$$

Substituting: - $V_{\text{ph–ph}} = 873\,\text{V}$ - $V_{\text{op,max}} = 900\,\text{V}$ - $\cos\varphi = 0.9$

We get:

$$I_{\text{rms,cond}} \approx 154.86 \cdot \sqrt{\frac{873}{900} \cdot \left(\frac{1}{2\pi} + \left(\frac{2}{\pi} - \frac{3 \cdot 873}{4 \cdot 900}\right) \cdot 0.9^2\right)} \approx 44.6\,\text{A}_{\text{rms}}$$

$$I_{\text{cond,pk}} = \sqrt{2} \cdot I_{\text{rms,cond}} \approx \sqrt{2} \cdot 44.6 \approx 63.1\,\text{A}_{\text{pk}}$$

Now that these current values have been determined, we calculate the required capacitance of the capacitor bank, assuming the worst-case electromagnetic scenario with a duty cycle of $D = 50\%$:

We compute the normalized ripple factor:

$$u = \frac{\Delta V_{\text{ripple,DC-link}}}{V_{\text{out,min}}} = \frac{8.99}{899} = 10^{-2}$$

$$C_{\text{des}} = 0.5 \cdot D \cdot (1 - D) \cdot \frac{I_{\text{cond,pk}}}{f_{\text{sw}} \cdot V_{\text{out,max}} \cdot u} = 0.5 \cdot 0.5 \cdot 0.5 \cdot \frac{63.1}{10\,000 \cdot 900 \cdot 10^{-2}} \approx 87.63\,\mu\text{F}$$

Capacitor Selection with Commercial Device

We now select a commercially available capacitor with a lower individual rating, to allow use of multiple identical units connected in parallel. The selected component is the Kemet C4AQOBW5360M3MJ, and its specifications are reported below.

Table 3.19: Capacitors specifications [17].

Producer	Kemet
Model	C4AQOBW5360M3MJ
Rated Voltage	900 V
Capacitance	36 μF
ESL	0.9 nH
ESR	2.1 mΩ
Weight	0.45 kg

To achieve the required total capacitance for the capacitor bank, 4 units will be connected 2 in parallel + a parallel of 2 in series . The resulting bank characteristics are reported in the following table.

Table 3.20: Capacitor banks specifications.

Rated Voltage	900 V
Capacitance $C_{DC,link}$	90 μF
ESL$_{\text{eq}}$	0.36 nH
ESR$_{\text{eq}}$	0.84 mΩ
Weight	1.8 kg

Resonance Check:

We verify that the system does not enter resonance by computing:

$$f_{\text{res}} = \frac{1}{2\pi\sqrt{ESL_{\text{eq}} \cdot C_{DC,link}}} = \frac{1}{2\pi\sqrt{5.2 \cdot 10^{-9} \cdot 90 \cdot 10^{-6}}} \approx 884.2\,\text{kHz}$$

Since $f_{\text{res}} > 3 \cdot f_{\text{sw}} = 30\,\text{kHz}$, the condition fully satisfied.

Power Losses:

Finally, we compute the power dissipated in the capacitor bank due to its ESR:

$$P_{\text{cap,losses}} = ESR_{\text{eq}} \cdot I^2_{\text{rms,cond}} = 0.00084 \cdot (44.6)^2 \approx 1.61\,\text{W}$$

Thus, the selected capacitor bank meets all functional and electrical requirements for the DC-link of the inverter system.

Capacitor Kemet C4AQOBW5360M3MJ

3.3.5 Sensors

Current Sensor

To monitor the inverter's output phase currents, a Hall-effect current sensor has been selected. This sensor is designed to accurately detect both AC and DC currents up to 500 A, making it well-suited for traction inverter applications in electric vehicles.

Its Hall-effect operating principle ensures galvanic isolation and a fast dynamic response, which makes it particularly suitable for high-frequency switching environments and secure signal acquisition.

Communication is handled via a CAN interface, allowing seamless integration with the vehicle control unit and eliminating the need for an external analog-to-digital conversion stage.

Table 3.21: Key specifications of the Hall-effect current sensor.

Parameter	**Value**
Current range	±500 A (AC/DC)
Frequency response	up to 50 kHz
Output	CAN interface / analog (with converter)

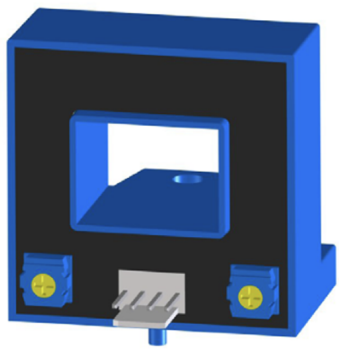

Figure 3.30: Hall-effect current sensor adopted for phase current measurement.

In addition to this external sensor, the inverter module (Infineon FS03MR12A6MA1LB) includes an integrated NTC thermistor for real-time junction temperature monitoring. This embedded sensing feature supports thermal protection and switching control optimization based on the actual temperature of the device.

Voltage Sensor

To perform isolated voltage measurements on the three-phase output of the inverter, the **LEM LV 25-P** transducer has been selected. This closed-loop Hall-effect device enables accurate sensing of AC, DC, and pulsed voltages, with galvanic separation between the primary and secondary circuits. These devices are essential to enable reliable motor control algorithmssuch as Field-Oriented Control (FOC)executed by the Vehicle Control Unit (VCU), and contribute to both system protection and diagnostics.

Operating Principle: A current proportional to the primary voltage is injected through an external resistor into the primary coil of the sensor. The device outputs a secondary current linearly scaled to the input voltage.

Table 3.22: Main characteristics of the LEM LV 25-P transducer [18].

Parameter	**Value**
Measurement range	10V to 500V (via external resistor)
Isolation voltage (1min, 50Hz)	2.5kV RMS
Impulse withstand voltage	16kV (1.2/50s)
Output signal	±25mA (nominal)
Supply voltage	±12V to ±15V
Total accuracy @25C	±0.8% (±0.9% typical)
Linearity error	<0.2%
Response time (90%)	40s
Operating temperature	0C to +70C
Mass	22g
Standards	EN50178, UL508

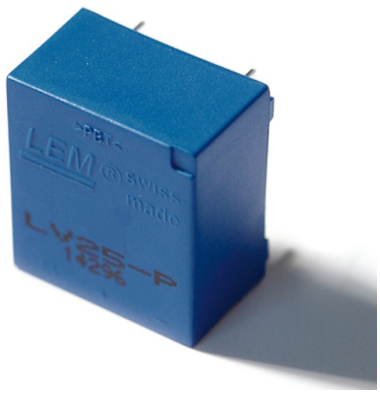

Figure 3.31: LEM LV 25-P Hall-effect voltage transducer.

Implementation Note: An external resistor R_1 is required to convert the voltage to a current in the primary circuit. The recommended design target is to generate 10mA primary current at nominal input voltage. For example:

$$R_1 = \frac{U_{PN}}{I_P} = \frac{250\,\mathrm{V}}{10\,\mathrm{mA}} = 25\,\mathrm{k}\Omega$$

This guarantees optimal accuracy with a total error of 0.9

The LV 25-P offers excellent immunity to electromagnetic noise, fast response time, and low offset, making it highly suitable for high-performance electric drives and power converters.

Traction Inverter Control Unit

The control of the traction inverter is based on Field-Oriented Control (FOC) combined with Space Vector Pulse Width Modulation (SVPWM), which allows efficient torque control and optimal use of the DC-link voltage.

To implement these real-time algorithms with high reliability and scalability, the **NXP S32K344** microcontroller has been selected. It belongs to the **S32K3** automotive-qualified family, featuring safety and security features compliant with ISO 26262 (up to ASIL D).

This device integrates a high-performance ARM Cortex-M7 core operating at up to 160 MHz, with an advanced set of peripherals optimized for powertrain applications, including FlexPWM and multiple 12/14-bit ADCs.

Figure 3.32: NXP S32K344 microcontroller for traction inverter control.

Table 3.23: Inverter control specifications [19].

Manufacturer	NXP Semiconductors
Microcontroller (32-bit)	S32K344
Core	ARM Cortex-M7
Clock Frequency	160 MHz
Flash Memory	up to 4 MB
SRAM	up to 1 MB
PWM channels	24 FlexPWM channels
ADC	Up to 4, 12/14-bit resolution
Communication Interfaces	3x CAN FD, SPI, I2C, UART, LIN
Supply Voltage	3.3 V
Functional Safety	ISO 26262 ASIL B/D
Operating Temperature	40 C to +150 C

The high level of integration and certified reliability of this microcontroller make it a suitable platform for traction inverter applications in electric vehicles, especially where modular control and safety compliance are required.

3.3.6 High Voltage to Low Voltage DC/DC Converter

Within the vehicle's electrical architecture, a robust and high-performance bidirectional DC/DC converter is required to interconnect the high-voltage (HV) and low-voltage (LV) systems. For this purpose, the **BrightLoop DCDC MO** unit has been selected, designed specifically for demanding applications such as motorsport and commercial electric vehicles.

This converter is based on an *isolated topology*, offering galvanic insulation tested up to 4000 VDC, and supporting both HV-to-LV and LV-to-HV energy flows. It provides one or two configurable LV outputs with up to 80 V each, and supports up to 300 A of continuous current. Its power delivery capabilities, reaching 6 kW, make it ideal for auxiliary loads such as pumps, ECUs, or low-voltage batteries.

Table 3.24: BrightLoop DCDC MO Key Specifications[20].

Parameter	**Specification**
HV input voltage	Up to 1000 V DC
LV output voltage	0–80 V DC (set via CAN)
LV current limit	Up to 300 A
Continuous output power	6000 W
Global efficiency	>94 %
HV/LV insulation	4000 V DC (60 s reinforced test)
Control interface	CAN bus (125 kbps to 1 Mbps)
Cooling method	Liquid-cooled (max 65 °C)
Environmental protection	IP68 / IP6K9K
Operating temperature	−40 °C to 80 °C
Dimensions (LWH)	164 mm 205.7 mm 50.3 mm
Weight	<4 kg

Figure 3.33: BrightLoop DCDC MO unit Electrical block diagram.

Thanks to its compact design, liquid cooling, and high environmental protection level (IP6K9K), the BrightLoop DCDC MO is ideal for onboard installation in harsh automotive environments. Its CAN interface allows full configurability of output voltage, current limits, and real-time monitoring of system parameters, including voltage, temperature, and fault status.

To meet the vehicle's auxiliary power needs, **two DCDC MO units** are used in parallel. One converter is dedicated to feeding the AC take-off system, while the second unit powers all remaining low-voltage devices, including the 12 V battery and safety-related electronics.

The power losses associated with the low-voltage grid can be estimated from:

$$P_{\text{losses}} = \frac{P_{\text{auxLV}}}{\eta_{\text{conv}}} \cdot (1 - \eta_{\text{conv}}) = \frac{6420}{0.94} \cdot (1 - 0.94) \approx 410\,\text{W}$$

The modular design also allows future expansion by configuring each LV port individually through the CAN interface, which is especially beneficial in dual-output applications.

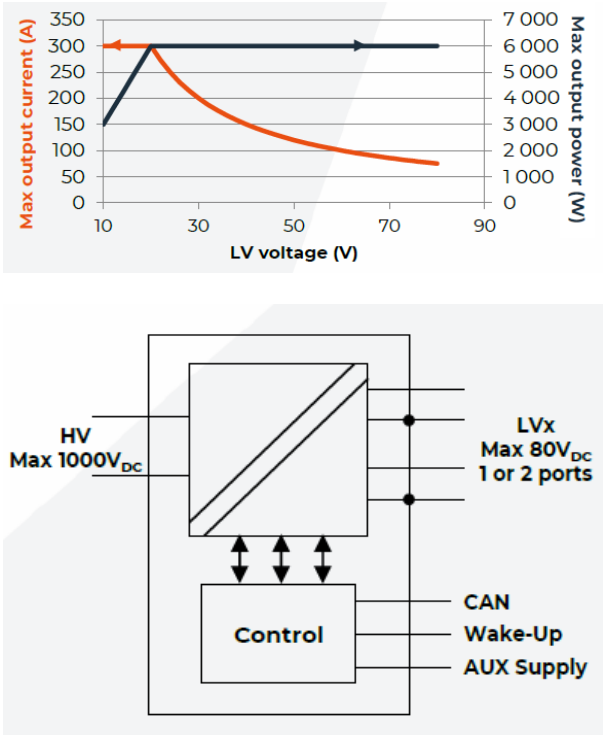

Figure 3.34: Electrical diagram and output performance of the DCDC converter

3.3.7 HV/HV DC/DC Converter for Battery Interface

To efficiently manage power flow between the traction battery and auxiliary high-voltage subsystems, a high-voltage isolated DC/DC converter is integrated. For this purpose, the **Fraunhofer IISB 22 kW DC/DC Converter** has been selected. This converter supports bidirectional power flow, making it suitable for both charging and discharging operations, energy buffering, and smart grid applications.

The converter is designed for systems with a nominal high-voltage battery around 900 V, and provides galvanic isolation, high switching frequency, and fast dynamic response. Its compact design and liquid cooling make it suitable for integration in automotive and industrial battery systems requiring high efficiency and robustness.

Table 3.25: Fraunhofer IISB 22 kW HV/HV DC/DC Main Specifications [21].

Parameter	**Value**
Power rating	22 kW (continuous)
Topology	Bidirectional isolated LLC
Input voltage range	100 V to 550 V
Output voltage range	450 V to 950 V
Switching frequency	250 kHz
Cooling method	Liquid cooling
Control interface	CAN bus
Dimensions (L W H)	340 190 130 mm
Weight	7.5 kg
Galvanic isolation	Reinforced, 3.5 kV DC

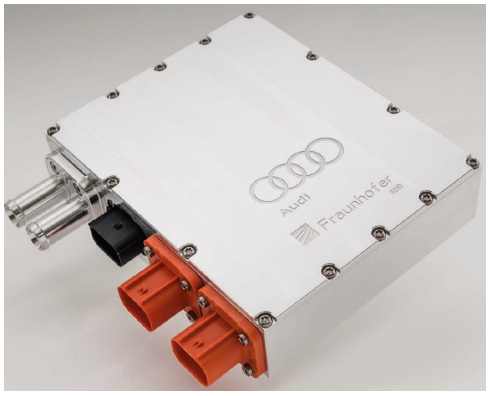

Figure 3.35: Fraunhofer IISB 22 kW bidirectional DC/DC converter.

Thanks to its high-frequency design and efficient liquid cooling, the converter achieves peak efficiencies exceeding 96 %, while maintaining a compact form factor. Its features enable advanced energy routing use cases such as high-voltage grid stabilization, dual-battery architectures, or onboard fast-charging modules. The CAN-based control interface ensures complete communication and diagnostics from the vehicle control unit.

3.3.8 On-Board Charger

The selected on-board charger (OBC) for this application is the **Innolectric MKI_OBC 22kW**. This system combines high charging performance with robust integration features, providing both AC and DC charging capabilities in a compact and rugged design.

The OBC supports three-phase AC charging with a nominal input of 400 V and can deliver up to 22 kW of power. The unit operates with a DC output voltage range from 220 V to 510 V, which is fully compatible with the high-voltage battery system of the vehicle. Efficiency exceeds 96 % for mid-range loads (210kW) and remains above 94 % at full load.

Thanks to its integrated liquid cooling system, CAN-based communication (including support for diagnostic and grid protocols such as ISO 15118 and DIN SPEC 70121), and high ingress protection (IP6K9K), the Innolectric OBC is particularly suited for automotive-grade environments and future grid-interactive applications such as V2G and V2L.

Table 3.26: Innolectric MKI_OBC Main Specifications [22]

Parameter	**Value**
Power rating	22 kW
Input voltage (AC)	400 V 10% (3-phase)
Input frequency	5060 Hz
Input current	Up to 32 A per phase
Output voltage (DC)	220 to 510 V
Output current	Up to 65 A
Efficiency (2 to 10 kW)	>96 %
Efficiency (full load)	>94 %
Cooling method	Liquid cooling
Ingress protection	IP6K9K
Communication	Dual CAN, ISO 15118, DIN SPEC 70121
Dimensions (L W H)	610 391 120 mm
Weight	30 kg
Operating temperature range	−40 to 65 °C

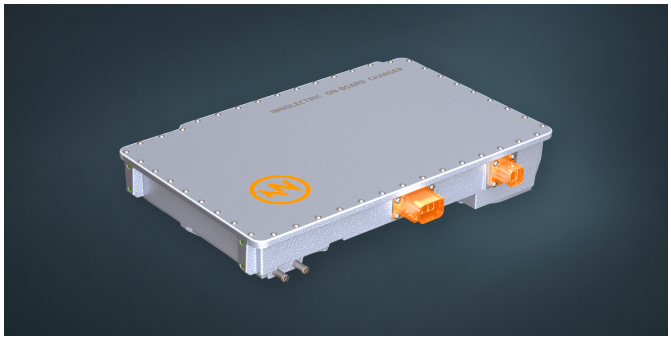

Figure 3.36: Innolectric MKI_OBC 22kW module.

To estimate the power losses during operation at full load, the following calculation is applied, considering a worst-case efficiency of 94%:

$$P_{\text{loss}} = P_{\text{OBC}} \cdot (1 - \eta_{\text{OBC}}) = 22000 \cdot (1 - 0.94) = 1320\,\text{W}$$

This value represents the thermal losses that must be managed by the cooling system under continuous charging conditions at maximum power.

3.4 Charging

Considering the charging method for the vehicle, there are mainly two: an AC charging and a DC one. Regarding the AC charging, an on-board charger presented in the previous paragraph is used; on the other hand for the DC charge an external charger is used to deliver power to the battery. For this reason, for the DC method we must provide only the suitable charging port. For the first charging method, we mentioned in the Chapter 2 the charging is performed at 22 kW and the charging time almost exceeds 10 hours.

$$\frac{E_{\text{batt}}}{P_{\text{charge}} \cdot \eta_{\text{charge}}} = \frac{200\,\text{kWh}}{22\,\text{kW} \cdot 0.95} = \frac{200}{20.9} \approx 9.57\,\text{hours}$$

The AC charging is Mode 3, for this reason an On Board Charger is required. This device consists of an AC/DC converter connected to the grid and an isolate DC/DC converter connected to the battery. For our specific case, another DC/DC converter after the OBC is required to match the voltage level of the battery. Below, a block scheme is represented:

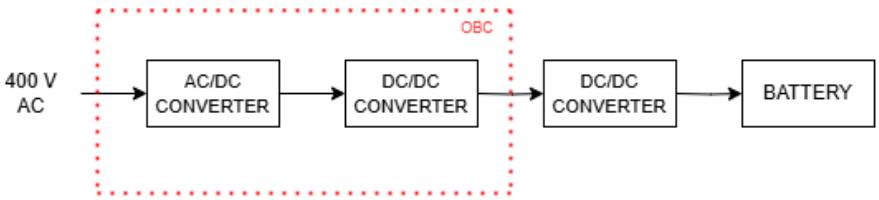

Figure 3.37: OBC block scheme

The chosen AC charging plug-in is the Phoenix Contact EV-T2AC-3P-32A-5.0M, which supports a three-phase 400 V supply with a maximum power of 22 kW. Moreover, this plug in allows to recharge the battery with private wall-box as well as the ones in the public stations.

Below, the main characteristics of the device are reported.

Table 3.27: Specifications of the AC charging plug-in (Type 2, Mode 3).

AC Plug-In	Phoenix Contact EV-T2AC-3P-32A-5.0M	
Max Current	32	A
Max Voltage	480	V
Phases	3	
Maximum Charging Power	22	kW

The chosen Socket is the CHARX connect universal CCS Type 2 charging socket from Phoenix Contact, specifically the model CHARX T2HBI12-3AC32DC250-2.0M2, which supports both three-phase AC charging at 22 kW and DC charging up to 250 kW.

Figure 3.38: Phoenix Contact EV-T2AC-3P-32A-5.0M Plug in [23]

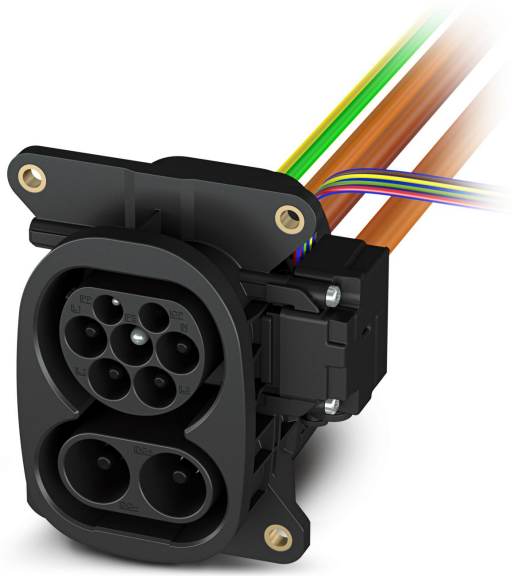

Figure 3.39: CHARX T2HBI12-3AC32DC250-2.0M2 Socket by Phoenix Contact [24]

Table 3.28: Socket Specifications

AC Charging Socket	Type 2 (IEC 62196-2)
Connection Method Precautions	Crimp connection; non-disconnectable
Max Current AC	32 A
Max Voltage AC	480 V
Phase	3 (Three-phase)
Maximum Charge Power AC	26.6 kW
Max Current DC	250 A
Max Voltage DC	1000 V
Maximum Charge Power DC	250 kW

3.5 Cooling circuit

The Hilux cooling system, as mentioned in the part 2, consists of two different circuits:

- **Low Temperature loop:** necessary to cool the battery pack, the on-board charger and the DC/DC converters.
- **High Temperature loop** which is then divided in two branches to include all four inverters and motors.

The HT (High Temperature) cooling loop is dedicated to components capable of operating under elevated thermal conditions. These elements can tolerate higher temperatures, allowing the loop to be optimized for efficient heat dissipation using a warmer coolant range.

On the other hand, the LT (Low Temperature) loop is designed for components with stricter thermal requirements. These systems, in particular the battery, require precise temperature regulation to maintain optimal performance within a narrow operating range. Below, the schemes of the two cooling loops are reported.

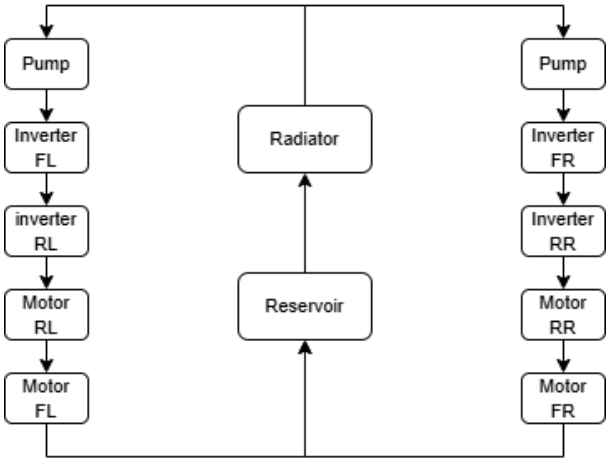

Figure 3.40: HT loop

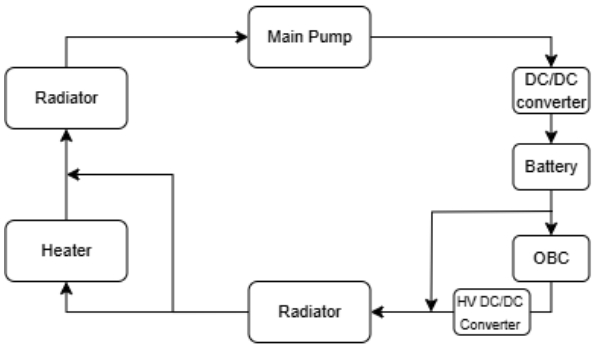

Figure 3.41: LT loop

On the LT loop, an heater is present that may be useful to warm the battery when temperatures are too low, ensuring optimal performance and protecting the battery from damage caused by cold conditions.

3.5.1 Low Temperature loop - Battery cooling

The topic analysed in this section, is related to the design of the low voltage cooling system. The fluid used in the cooling system is water and glycol, in equal parts and considering a worst condition (35C). To find the value of the losses, the expected efficiency of the Part 1 has been considered.

Property	**At 20C**	**At 35C (estimated)**
Density (kg/m^3)	1042	∼1035
Specific heat (J/kg·K)	3290	∼3180

Table 3.29: Specifications for water-glycol at 35°C.

The expected efficiency for the battery pack in the first part of the report, has been estimated equal to 17 kW, considering the maximum power derivable at the wheels.Considering the losses of the other components of the LT loop we reach a power that needs to be cooled of 19.5 kW. Now, it is possible to find from this introduction the value of flow-rate necessary to cool down the battery pack.

$$W = c_p \cdot \rho \cdot \dot{V} \cdot \Delta T \simeq 19000 \text{ W}$$

$$\dot{V} = \frac{W}{c_p \cdot \Delta T \cdot \rho} \cdot 60 \cdot 1000 = \frac{19000}{3176 \cdot 25 \cdot 1034.8} \cdot 60 \cdot 1000 \approx 13.9 \text{ l/min}$$

Now, it is necessary to select the correct hydraulic cooling pump which needs to be suitable to satisfy the flow rate and the supply voltage level available from the DC/DC converter. The chosen model is the one produced by SPAL, in particular, their 12 V brushless cooling pump.

Table 3.30: Cooling Pump Specifications SPAL 12V

Cooling Pump	SPAL Brushless Coolant Pump
Supply voltage	12 V
Current consumption	510 A (typical)
Flow rate	up to 15 l/min
Maximum pressure	1.0 bar
Weight	0.8 kg

Figure 3.42: SPAL 12V Brushless cooling pump

The selected model is capable of operating at a flow rate higher than the necessary one considering the total pressure drop in the cooling loop. At 1.0 bar, the pump is able to reach 15 l/min.

Considering the high flow rate value obtained, which is considerably higher than necessary for the DC/DC converter, the on-board charger and the LV DC/DC converter, it is necessary to position these three devices on three parallel paths. By doing so, we are able to achieve a reduced flow rate that passes through them.

The following table summarizes the delta temperatures for each element of the loop.

Table 3.31: Inlet and outlet temperatures for each component of the LT loop

Component	**Losses (kW)**	**Inlet (C)**	**Outlet (C)**
DC/DC Converter	0.3	25.0	25.4
Battery	17	25.4	46.6
On-Board Charger	1.2	46.6	48.1
HV DC/DC Converter	0.8	48.1	49.2 (reset)
Radiator	-	Reduce Temperature	to 25C

To conclude this subsection, it is necessary to explain more details about the battery pack cooling. The cells are placed vertically next to each other, forming the module. To cool them, cooling plates are placed above and below the cells to achieve a more uniform temperature distribution. Considering the characteristics of the selected pump, we cannot use only two cold plates per module and connect them all in series. Instead, we are still going to use two cold plates per module (one on top and the other on the bottom), but instead of connecting them all in series, we are going to use four branches in parallel, and for each branch, three modules will be connected in series. In doing so, we are able to contain the pressure drop below 0.75 bar and the cooling for each branch is still below the limit of ΔT equal to or below 25 C. This condition is verified by means of the following formulas, starting from the calculation of the power that needs to be dissipated by each branch.

$$Q_{\text{branch}} = \frac{Q_{\text{total}}}{N_{\text{branches}}} = \frac{17{,}000}{4} = 4250\,\text{W}$$

Now we calculate the flow rate for each branch and then convert it in kilograms per meter.

$$\dot{V}_{\text{branch}} = \frac{\dot{V}_{\text{total}}}{N_{\text{branches}}} = \frac{12.41}{4} = 3.10\,\text{l/min}$$

$$\dot{m}_{\text{branch}} = \dot{V}_{\text{branch}} \cdot \frac{\rho}{60 \cdot 1000} = 3.10 \cdot \frac{1034.8}{60{,}000} \approx 0.0536\,\text{kg/s}$$

And finally, we find the ΔT per branch.

$$\Delta T = \frac{Q_{\text{branch}}}{\dot{m}_{\text{branch}} \cdot c_p} = \frac{4250}{0.0536 \cdot 3176} \approx 24.9\,°\text{C}$$

As it is possible to appreciate from these calculations, this configuration is able to satisfy our requirements. Below, a simple cooling scheme is reported to better understand the configuration used.

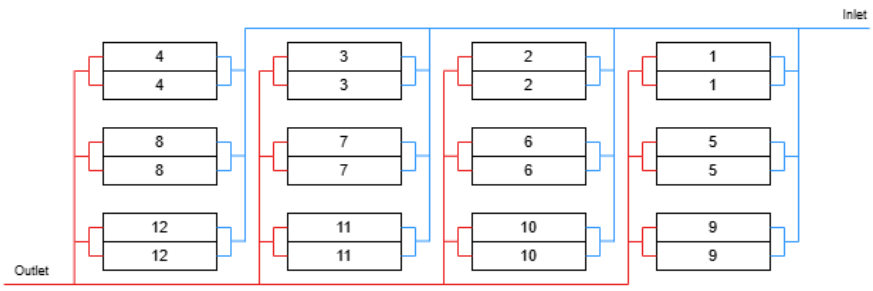

Figure 3.43: Top view of cold plates configurations for battery modules

3.5.2 High Temperature loop - Inverters and motors cooling

Considering the high temperature loop, we sad before that we have two separate branches which will be "supplied" by two separate pumps. Considering the efficiencies from the Part 1, the maximum power losses per each branch stands around 12 kW. Considering the efficiencies of the two motors and the two inverters it is possible to find the value of flow rate following the same steps performed for the low temperature loop.

$$W = c_p \cdot \rho \cdot \dot{m} \cdot \Delta T \simeq 18000\,\mathrm{W}$$

$$\dot{V} = \frac{W}{c_p \cdot \Delta T \cdot \rho} \cdot 60 \cdot 1000 = \frac{18000}{3176 \cdot 30 \cdot 1034.8} \cdot 60 \cdot 1000 \approx 10.96\,\mathrm{l/min}$$

Below, the inlet and outlet for a single branch are reported.

Table 3.32: Component Temperatures in the HT Loop (Starting at 40 C)

Component	**Losses (kW)**	**Inlet (C)**	**Outlet (C)**
Inverter 1	3.30	40.00	45.48
Inverter 2	3.30	45.48	50.95
Motor 2	6.00	50.95	60.91
Motor 1	6.00	60.91	70.87
Radiator	–	Reduce Temperature	to 40 C

Since the HT loop consists of two separate branches, two pumps need to be used. Considering the flow rate level calculated, it is possible to use the same pump chosen for the LT loop. Below the cold plate chosen to cool down the power modules is reported. The cold plate has been chosen compatibly with the power module dimensions.

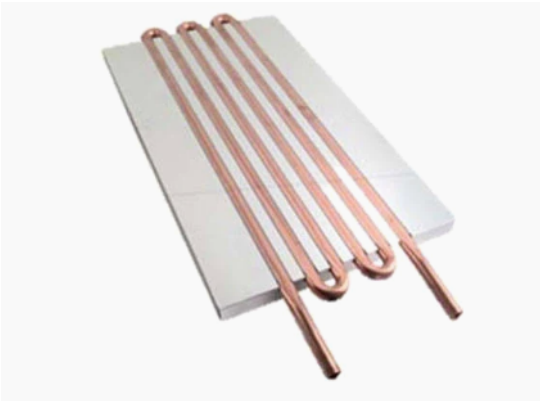

Figure 3.44: Liquid cooling plate for the inverters power modules[25]

Table 3.33: Aluminum plate for the cooling of the power switches

Product name	Boyd Laconia 416101U00000G
Material	Aluminum Alloy
Dimension	233.4 mm × 177.8 mm × 16.3 mm
Thermal Resistance	0.010°C/W at 1.5 GPM
Pressure Drop	0.827 bar at 9.5 l/min

In conclusion, it is necessary to spend few words about the configuration chosen. In particular, it has been chosen to cool down first the two inverters and then the motors. This choice has been led by the narrower operating temperature range that the inverter are able to work within. Moreover, in this way we are able to "close" the cooling loop optimizing the pipe lengths throughout the whole system. Below, a schematic that represents the HT loop is reported.

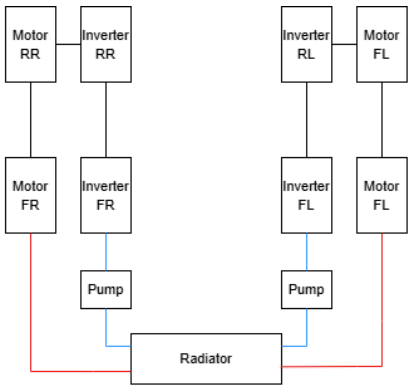

Figure 3.45: Top view of HT cooling loop configuration in the vehicle

Bibliography

[1] Toyota Motor Corporation. Toyota hilux scheda tecnica. URL: https://www.toyota.it/content/dam/toyota/nmsc/italy/gamma/pdf/scheda-tecnica/HILUX_scheda-tecnica.pdf.

[2] Samsung. Sdi 21700-50e datasheet. URL: https://asset.conrad.com/media10/add/160267/c1/-/en/002114678DS01/scheda-tecnica-2114678-samsung-inr21700-50e-batteria-ricaricabile-speciale-21700-pdf.

[3] Mersen. Mdc10m400b datasheet. URL: https://www.mersen.com/sites/default/files/medias/PIM/files/DS-MDC10M-1000VDC-Main-DC-Distribution-Fuse-Mersen-EN.pdf.

[4] Sensata Technologies. Gvb351bax datasheet. URL: https://www.sensata.com/sites/default/files/a/sensata-gigavac-GVB35-series-contactor-datasheet.pdf.

[5] TE Connectivity. Powertube 1400 datasheet. URL: https://www.te.com/content/dam/te-com/documents/industrial-and-commercial-transportation/global/ict-powertube-ds-a4-en.pdf.

[6] Isabellenhutte. Ivt-s datasheet. URL: https://www.isabellenhuetteusa.com/wp-content/uploads/2022/07/Datasheet-IVT-S-V1.03.pdf.

[7] Bender. Isometer ir155 datasheet. URL: https://www.bender.de/fileadmin/content/Products/d/e/IR155-32xx-V004_D00115_D_XXEN.pdf.

[8] Orion. Orion bms 2 datasheet. URL: https://www.orionbms.com/downloads/documents/orionbms2_specifications.pdf.

[9] TE Connectivity. Hsa50180rj resistor datasheet. URL: https://www.te.com/en/product-1-1625984-3.datasheet.pdf.

[10] Brusa Elektronik. Hsm2-10.18.22 datasheet. URL: https://www.brusatechnology.com/portfolio/hsm2-10-18-22/.

[11] Tamagawa Seiki Co., Ltd. Smartsyn brushless resolver datasheet. URL: https://www.tamagawa-seiki.com/products/resolver-synchro/brushless-resolver-smartsyn-builtin.html.

[12] Renhotec EV. 150mm 1500v 430a highvoltage ev cable datasheet. URL: https://www.renhotecev.com/product/1500v-430a-high-voltage-unshielded-ev-cable-150mm2-energy-storage-system-cable.

[13] Leoni AG. Dacar power cable datasheet. URL: https://www.hbcables.com/app/uploads/2019/02/Leoni-Dacar.pdf.

[14] Infineon Technologies AG. Fs03mr12a6ma1lb silicon carbide power module. URL: https://www.infineon.com/cms/en/product/power/mosfet/silicon-carbide/modules/fs03mr12a6ma1lb/.

[15] KEMET Corporation. C4aqolu4250p12j film capacitor datasheet. URL: https://www.digikey.be/en/products/detail/kemet/C4AQOLU4250P12J/14010079.

[16] Magnetics A Division of SPang Co. 0w42616ug power inductor datasheet. URL: https://www.digikey.cn/en/products/detail/magnetics-a-division-of-spang-co/0W42616UG/21221128.

[17] KEMET Corporation. C4aqobw5360m3mj film capacitor datasheet. URL: https://www.digikey.it/it/products/detail/kemet/C4AQOBW5360M3MJ/13563412.

[18] LEM SA. Lv25p current transducer datasheet. URL: https://www.lem.com/en/product-list/lv-25p.

[19] NXP Semiconductors. S32k3 automotive generalpurpose mcu family datasheet. URL: https://www.nxp.com/products/S32K3.

[20] BrightLoop Converters. Dcdc mo hvlv dc/dc converter datasheet. URL: https://brightloop.fr/products/hv-lv-dc-dc-converters/dcdc-mo/.

[21] Fraunhofer IISB. 22 kw 900 v dc/dc converter datasheet. URL: https://www.iisb.fraunhofer.de/content/dam/iisb2014/en/Documents/Research-Areas/power_electronics/22-kW-900-V-DCDC-Converter_FraunhoferIISB_1V5_WWW.pdf.

[22] Innolectric AG. Onboard charger2.2 datasheet. URL: https://innolectric.ag/on-board-charger-2-2/?lang=en.

[23] Phoenix Contact GmbH Co. KG. Cavo di ricarica ac ev t2 g3 pc 3ac32a 60esbk01. URL: https://www.phoenixcontact.com/it-it/prodotti/cavo-di-ricarica-ac-ev-t2g3pc-3ac32a-50m60esbk01-1627692.

[24] Phoenix Contact GmbH Co. KG. Charx t2hbi123ac32dc2502.0m2 vehicle charging inlet (ccs type2, 250adc / 32aac). URL: https://www.phoenixcontact.com/en-us/products/vehicle-charging-inlet-charx-t2hbi12-3ac32dc250-20m2-1162095.

[25] Boyd. Boyd coldplate heat sink. URL: https://info.boydcorp.com/hubfs/Thermal/Liquid-Cooling/Boyd-Hi-Contact-6-Pass-Datasheet.pdf.